Nat. Hazards Earth Syst. Sci., 13, 1527–1549, 2013
www.nat-hazards-earth-syst-sci.net/13/1527/2013/
doi:10.5194/nhess-13-1527-2013

Natural Hazards and Earth System Sciences
Open Access

The combination of DInSAR and facility damage data for the updating of slow-moving landslide inventory maps at medium scale

L. Cascini[1], D. Peduto[1], G. Pisciotta[2], L. Arena[1], S. Ferlisi[1], and G. Fornaro[3]

[1]Department of Civil Engineering, University of Salerno, Via Giovanni Paolo II, 132, 84084 Fisciano (Salerno), Italy
[2]Via Ventaglieri, 77, 80135 Naples, Italy
[3]Institute for Electromagnetic Sensing of the Environment (IREA–CNR), Via Diocleziano 328, 80124 Naples, Italy

Correspondence to: D. Peduto (dpeduto@unisa.it)

Received: 19 December 2012 – Published in Nat. Hazards Earth Syst. Sci. Discuss.: –
Revised: 15 April 2013 – Accepted: 30 April 2013 – Published: 18 June 2013

Abstract. Testing innovative procedures and techniques to update landslide inventory maps is a timely topic widely discussed in the scientific literature. In this regard remote sensing techniques – such as the Synthetic Aperture Radar Differential Interferometry (DInSAR) – can provide a valuable contribution to studies concerning slow-moving landslides in different geological contexts all over the world. In this paper, DInSAR data are firstly analysed via an innovative approach aimed at enhancing both the exploitation and the interpretation of remote sensing information; then, they are complemented with the results of an accurate analysis of survey-recorded damage to facilities due to slow-moving landslides. In particular, after being separately analysed to provide independent landslide movement indicators, the two datasets are combined in a DInSAR-Damage matrix which can be used to update the state of activity of slow-moving landslides. Moreover, together with the information provided by geomorphological maps, the two datasets are proven to be useful in detecting unmapped phenomena. The potentialities of the adopted procedure are tested in an area of southern Italy where slow-moving landslides are widespread and accurately mapped by using geomorphological criteria.

1 Introduction

A fundamental step in the landslide risk analysis and, more generally, in the landslide risk management process (Fell et al., 2008a) is represented by landslide inventory mapping which usually includes location, classification, volume, state of activity, date of occurrence (if available) and other characteristics of landslides. Accordingly, the obtained maps need to be not only accurate but also updated on a regular basis.

The scientific literature is very rich of methodologies for landslide inventory mapping (Wieczoreck, 1984; Soeters and van Westen, 1996; Malamud et al., 2004; van Westen, 2004; van Westen et al., 2008). On this topic, Guzzetti et al. (2012) recently provided a comprehensive review focusing on the use of both conventional and new technologies for the production of landslide inventory maps, highlighting that this activity still relies chiefly on the visual interpretation of stereoscopic aerial photography aided by field surveys. However, due to the high costs in terms of both time and money necessary for their fulfillment new technologies need to be increasingly used.

In this regard, remote sensing techniques can offer a valuable contribution, as it is testified by the rapidly growing number of scientific works dealing with landslide inventory mapping achieved by means of the analysis of the information gathered by either passive or active air- and space-borne sensors or the integration of traditional ground-based monitoring with remote sensing data (Catani et al., 2005; Nichol and Wong, 2005; Van den Eeckhout et al., 2007; Tofani et al., 2013). In particular, as it is pointed out in the report "Deliverable 4.4" (SafeLand Deliverable 4.4, 2011) of the EU-funded SafeLand Project (http://www.safeland-fp7.eu), Synthetic Aperture Radar Differential Interferometry (DInSAR) techniques may represent suitable tools for updating inventory maps dealing with slow-moving landslides, namely mass movement phenomena whose typical velocity values range from few $\mathrm{mm\,yr^{-1}}$ up to $1.6\,\mathrm{m\,yr^{-1}}$ (Cruden

and Varnes, 1996). This kind of phenomena is widespread all over the world and systematically cause significant damages to structures and infrastructures (D'Elia and Rossi-Doria, 2000; Picarelli and Russo, 2004; Spizzichino et al., 2004; Bonnard et al., 2008; Wang et al., 2008; Urciuoli and Picarelli, 2008; Mansour et al., 2011) requiring high costs for rehabilitation, securing and maintenance.

Focusing on slow-moving landslides involving urbanised areas of central-southern Italian Apennines (Bertolini et al., 2005; Cotecchia, 2006; Cascini et al., 2008; Guzzetti et al., 2008; Cotecchia et al., 2008), Cascini et al. (2008) discussed the possibility to update available inventory maps through the integration of remote sensing data, thematic maps and damage surveys to structures/infrastructures. Indeed, landslide-induced damages – whether available – can be considered as movement indicators and, thus, can be used to validate DInSAR data where both datasets are available (e.g. in urbanised areas) as well as to overcome any lacks of remote sensing data availability (e.g. over vegetated areas).

The main purpose of this paper is to present a new methodology that improves the exploitation of the abovementioned datasets for a study area of southern Italy thus allowing the updating of slow-moving landslide inventory maps at medium scale (1 : 25 000) with reference to both the state of activity and the detection of unmapped phenomena. The adopted approach although suited for the available datasets can be valuably exported in different geological contexts using similar data.

2 Study area and landslide inventory

The study area (557 km^2) is located in the south-east part of National Basin Authority of Liri-Garigliano and Volturno rivers (NBA LGV) and includes 21 Municipalities and 2 Provinces (Benevento and Avellino) belonging to the Campania region in southern Italy (Fig. 1). This area was selected due to the widespread distribution of slow-moving landslides (covering around 25 % of the total extension) which caused losses to structures/infrastructures interacting with them (Melidoro, 1971; D'Elia et al., 1985; Budetta et al., 1994; SCAI Project, 2004; Guadagno et al., 2006; APAT, 2007; Cascini et al., 2008).

For the study area, base (topographic) maps at 1 : 5000 scale and thematic (geological, geomorphological, landslide inventory) maps at 1 : 25 000 scale are available. These maps were developed during the activities carried out by the NBA-LGV within the PsAI-Rf (Hydrogeological Setting Plans – Landslide Risk excerpt) project (Italian Law 365/2000).

In particular, the geological map of the area highlights the existence of Mesozoic–Tertiary lithological units mainly consisting of clayey-sandy-arenaceous and clayey-calcareous-siliceous strata covered by marly-calcareous, arenaceous and arenaceous-conglomeratic units (Rapolla et al., 2012). These latter units together with the geostructural

Fig. 1. The study area.

setting mainly control the geomorphological features of the area.

As for landslide inventory (Fig. 2), the available map – developed at 1 : 25 000 scale on the basis of geomorphological criteria supported by field survey data and aerial photo interpretation – furnishes detailed information for each mapped phenomenon with reference to location, type, state of activity and areal extension.

As far as the type of phenomenon is concerned (over a total number of 2180 slow-moving landslides) the inventory map distinguishes: 766 rotational slides; 267 rotational slide–earth flows; 1117 earth flows; 30 deep-seated gravitational movements (dsgm); moreover, 158 creep phenomena, 65 earth flow-creeps and 2 rotational slide-creeps are also inventoried (Fig. 3a–b). Furthermore, according to the adopted approach for landslide inventory mapping, two possible states of activity for rotational slides, rotational slide-earth flows and earth flows are considered (Fig. 3a): "dormant" landslides and "active" landslides, the latter including active, reactivated and suspended phenomena (Cruden and Varnes, 1996). On these bases, Fig. 3a shows a predominance of dormant phenomena (1562) on active ones (588) with size ranging from around 0.1 ha up to around 200 ha (Fig. 3b).

3 The data used for landslide inventory updating

3.1 The DInSAR techniques

Since early 2000s multi-pass DInSAR algorithms have been widely used to retrieve information on displacements of the topographic surface. The available techniques for the analysis of phase signals in interferometric stacks can be grouped in two classes: persistent scatterers interferometry (PSI) (Ferretti et al., 2000, 2001; Costantini et al., 2008; Crosetto et al., 2008) and Small-Baseline (SBAS) approaches (Berardino et al., 2002; Fornaro et al., 2009a). In the first class, the analysis is carried out at full resolution on stable

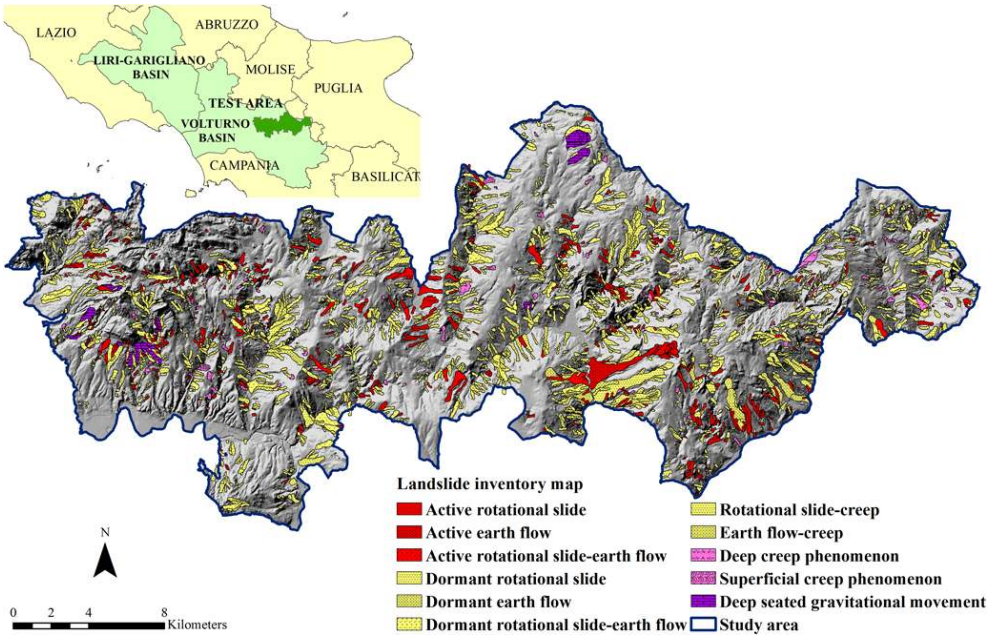

Fig. 2. Distribution and types of slow-moving landslides over the study area.

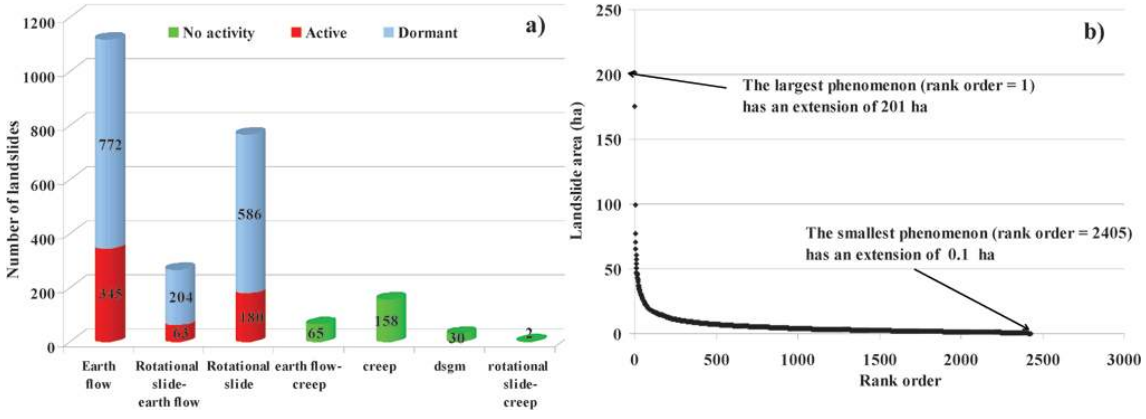

Fig. 3. (a) Number and state of activity of mapped phenomena distinguished per types within the test area; **(b)** distribution of slow-moving landslide extension within the test area.

scatterers in order to separate the atmospheric, topographic and deformation components. In the case of SBAS techniques, the scattering is supposed to be distributed within the resolution cell and spatial multilooking is implemented to enhance the phase stability. As a consequence of this operation, the spatial resolution of the product is degraded with respect to the PSI approach. Nevertheless, a side product of the small scale analysis is the estimate of the atmospheric phase delay (APD) which allows the implementation of a subsequent large scale analysis carried out at full-resolution (Fornaro et al., 2009b).

In parallel to the two-step interferometric analyisis based on low (Berardino et al., 2002; Fornaro et al., 2009a) and full resolution (Fornaro et al., 2009b) processing, an upgrading of the PSInSAR technique (Ferretti et al., 2000, 2001), which also makes use of multilooking during the data processing, known as SQUEESAR (Fumagalli et al., 2011), has been recently developed for the monitoring also of distributed scatterers.

The dataset used in this paper derives from the application of the PSI technique (Ferretti et al., 2001; Costantini et al., 2008) belonging to the first group of algorithms. Persistent scatterers (PS) can be identified as a subset of coherent radar targets usually coinciding with man-made structures (buildings, roads, etc.) and natural targets (e.g. bare rocks) on the ground. PS-derived velocity is acquired along the radar line of sight (LOS) with reference to a fixed point on the ground (reference point) and with an accuracy of $\pm 1\,\mathrm{mm\,yr^{-1}}$ for

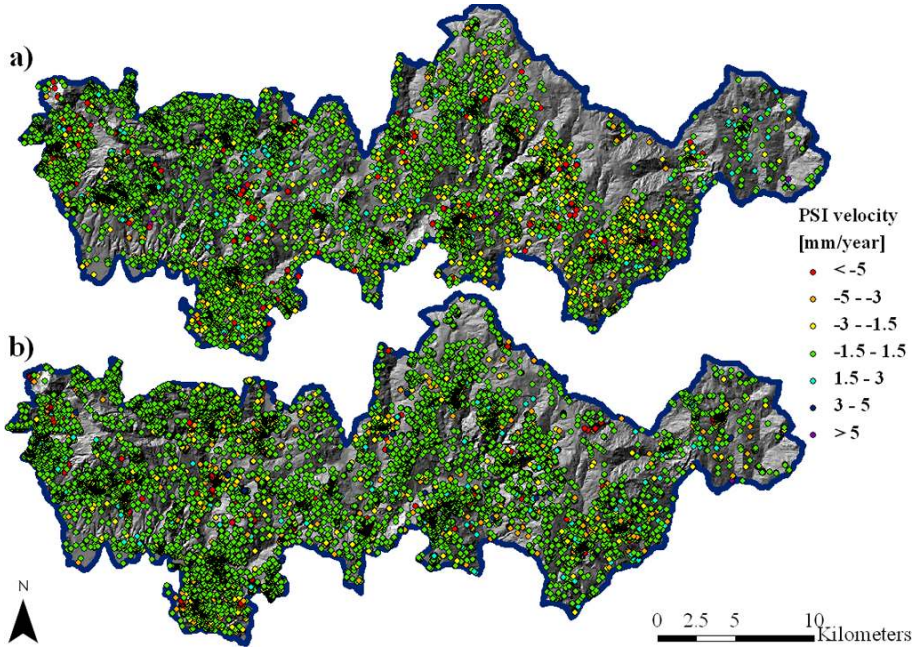

Fig. 4. Distribution of PSI data over the study area according to **(a)** ERS and **(b)** ENVISAT sensor.

the average velocity and ±5 mm on the single displacement measure. Each PS is associated with a coherence value (ranging from 0 up to 1) which indicates how the measure fits the model assumed for the displacement.

In the scientific literature several papers deal with the application of PSI – and more generally DInSAR – techniques to the study of slow-moving landslides. These works highlight the potential of the techniques as well as the current limits essentially related to (i) sensor revisiting times which allow the collection of information with reference to landslides whose velocity – according to classes provided by Cruden and Varnes (1996) – ranges from extremely slow to very slow (Colesanti and Wasowski, 2006; Cascini et al., 2009, 2010); (ii) very low coverage on vegetated areas for sensors operating at C band (Wei and Sandwell, 2010); (iii) 1-D LOS measurements which call for necessary projection operations taking into account: slope and aspect angles; the acquisition geometry of the sensors; and the kinematic features of the observed phenomenon (Colesanti and Wasowski, 2006; Cascini et al., 2009, 2010).

Up to now the use of DInSAR data for slow-moving landslide characterization and mapping has been investigated in several studies carried out at different scale of analysis (Fell et al., 2008a): small (<1 : 100 000) (Meisina et al., 2008); medium (1 : 100 000 to 1 : 25 000) (Catani et al., 2005; Cascini et al., 2009, 2010; Lu et al., 2012); large (1 : 25 000 to 1 : 5000) (Notti et al., 2010) and detailed (>1:5000) (Colesanti et al., 2003; Herrera et al., 2011).

Moreover, the types of slow-moving landslides (Varnes, 1978) investigated by DInSAR data analyses in the aforementioned studies are mainly: slides and earth flows, deep-seated gravitational movements and creep phenomena (Tofani et al., 2013).

The PSI data used for the present study were collected within the Piano Straordinario di Telerilevamento (MATTM, 2010) which is a project supported by the Italian Ministry of the Environment and Protection of Land and Sea covering all the Italian territory with an ERS-ENVISAT sensor database of almost 20 yr since 1992. In particular, for the study area the following data are available: 208 ERS images on ascending orbit (period September 1992–September 2000) and 134 on descending orbit (period November 1992–December 2000); 52 ENVISAT images on ascending orbit (period November 2002–July 2010) and 49 on descending orbit (period March 2003–June 2010). The distribution and the recorded velocity of both ERS and ENVISAT PS over the study area are shown, respectively, in Fig. 4a and b. ERS data exhibit a density of 43.4 PS km^{-2}, whereas a density equal to 91.4 PS km^{-2} is recorded for ENVISAT data.

This project together with other international (TERRAFIRMA, 2012; DORIS, 2012), national and regional projects (Meisina et al., 2008; Terranova et al., 2009; Risknat Project, 2012) in different countries provides end-users with a huge database, thus stressing the importance of the development of standard procedures for the appropriate analysis and interpretation of remote sensing data. This issue is addressed in the next sections with reference to the possibility of integrating these data with both damage survey data and landslide inventory maps.

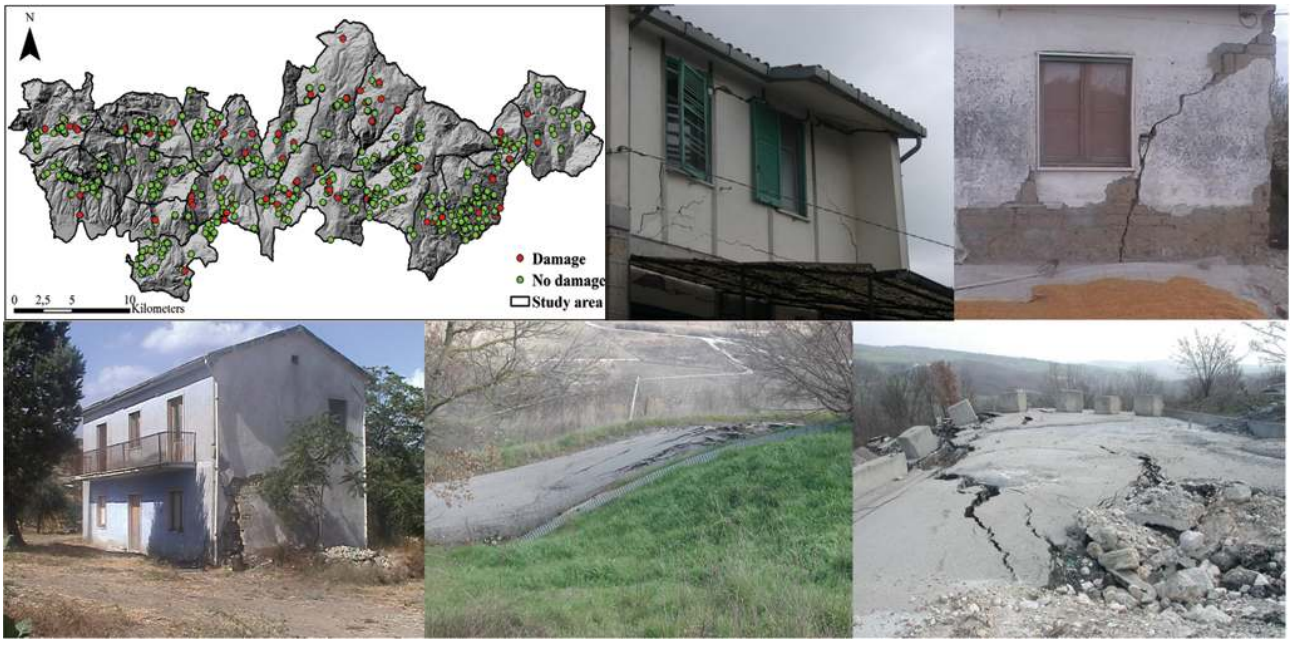

Fig. 5. Distribution of landslide-induced damages within the test area and some examples of damages recorded to buildings and roads.

3.2 Facility damage dataset

The damage analysis of buildings and/or roads interacting with slow-moving landslide bodies is a difficult task because it requires a deep knowledge of relevant factors related to both landslides (type, intensity, etc.) and exposed facilities (materials, state of maintenance, foundation type, etc.) as well as information on their relative location within the landslide affected area (Cascini et al., 2005; Fell et al., 2008b). In order to overcome this difficulty, the problem can be addressed empirically by collecting reliable data on landslide-induced damages (Leone et al., 1996) as in the case of the study area where damage information on 1035 facilities (buildings and roads) is available (Fig. 5). These data were recorded in 2000 via surveys carried out by experts and technicians involved in the activities of the NBA-LGV within the PsAI-Rf project. The gathered information was reported in fact sheets and includes the landslide type; the characteristics of the exposed facility and its relative location within the landslide affected area; the occurrence date of the damage (if any); the structural (e.g. columns and beams for reinforced concrete buildings) or non-structural (e.g. infill walls) damaged elements; the state of maintenance and other additional information, such as the damage recurrence (if any) on the exposed facility (mainly roads).

In this work, according to the definitions provided by the Ministerial Decree issued on 14 January 2008 by the Italian Ministry of Infrastructure and Transport, damages whose severity corresponds – for a given facility – to the attainment of a Serviceability Limit State (e.g. loss of functionality) or an Ultimate Limit State (e.g. partial collapse of a superstructure) were considered for the purpose of the analysis. Totally, 212 damaged facilities (among which 44.8 % are buildings and 55.2 % correspond to roads) were inventoried in the study area.

4 The approach adopted at 1 : 25 000 scale

The adopted approach consists of four phases to be carried out separately for the analysis of DInSAR and damage data which both play as ground movement indicators (Fig. 6). After these phases, the two analysed datasets are merged into a DInSAR-Damage matrix which provides the updated state of activity as output. Hereafter, the procedures applied for the analysis of the two datasets are described in detail.

4.1 The procedure for the analysis of DInSAR data

The first phase (Fig. 6) includes the generation of the a priori landslide visibility map introduced by Cascini et al. (2009) (see also Plank et al., 2010), allowing the identification of the landslide affected areas for which radar ground targets can be detected prior to the SAR image processing. To this aim the map is generated through the joint use of a digital elevation model (DEM) of the area and its derivatives (slope and aspect angle) as well as the land-use map and the sensor acquisition geometry. In the a priori landslide visibility map the nonlinear effects related to topography (i.e. shadowing) are disregarded, thus visible areas may be overestimated.

Then, a new index is introduced, referred to as A-Index, which can be computed for each PS time series in order to complement with the velocity value for the definition of

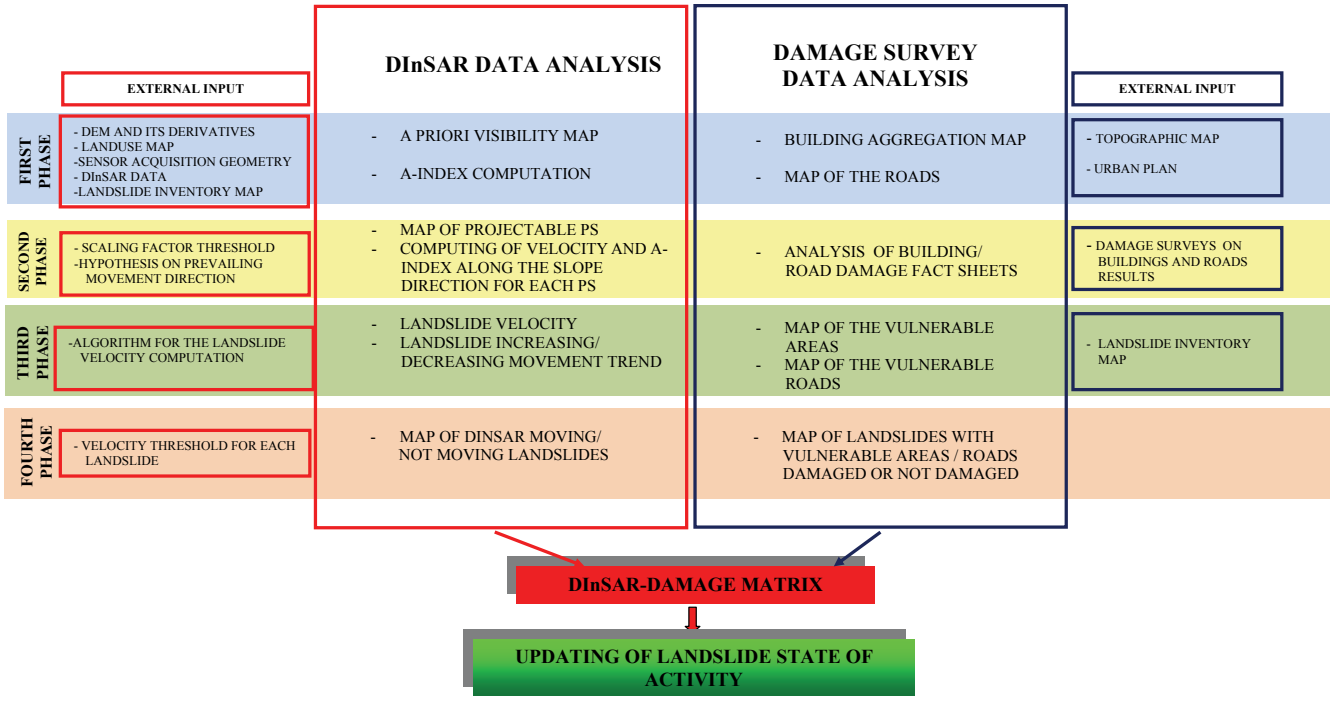

Fig. 6. Flow-chart describing the procedure adopted for the updating of the state of activity of slow-moving landslides.

landslide state of activity. In particular, the A-Index represents the second order derivative of the second order polynomial curve best fitting the PS displacement time series (see Fig. 7a). The combination of the velocity value and the A-Index of each PS can provide useful information on the trend of measured displacements. In particular, as it is shown in Fig. 7b for a sample dataset, when the signs of the A-Index and the velocity are concordant (i.e. both negative or positive) the trend of the time series can be considered as increasing; on the other hand, discordant signs of A-index and velocity values (i.e. positive and negative) represents decreasing displacement trends. In the same figure the occurrence in log-scale of the couples velocity A-Index is shown.

In Sect. 4.3 the improvement of DInSAR data interpretation via the advanced exploitation of PS time series will be highlighted. This issue up to now has been only partially achieved in the scientific literature (Cigna et al., 2011).

The quantitative analysis and interpretation of 1D-LOS DInSAR data is closely related to the value of velocity/displacement along a given movement direction. To address this issue in the second phase, due to the scale of the analysis, firstly a prevalent translational movement along the steepest slope direction is assumed for each PS according to Cascini et al. (2010). Considering that the LOS projection on the along-slope direction can be biased by errors related to the projection operation (Colesanti and Wasowski, 2006; Cascini et al., 2010), the map of projectable DInSAR data is introduced (Plank et al., 2010). This map distinguishes each PS according to the own scaling factor, namely the constant value by which the modulus of the LOS velocity (V_{LOS}) must be multiplied in order to obtain the modulus of the along-slope velocity (V_{slope}). This issue was already addressed by Cascini et al. (2010) through the adoption of the condition number of the inversion matrix solving the algebraic system used for the projection operation (i.e. from ascending, or descending, or ascending-descending LOS to slope direction). Indeed, the condition number is a measure of the instability of the inversion process and, in particular, of the accuracy of the solution after the inversion process. As shown by the authors, values of the condition number not exceeding 15 could be an acceptable threshold to select the most reliable projected PS velocity values. Figure 8 shows that the above-mentioned threshold also corresponds, in the case of data acquired on single orbits (either ascending or descending), to those values of the scaling factor not exceeding 3.3 for the selected study area. This threshold, which avoids the use of unreliable PS velocity, also matches with those assumed in other published researches (Plank et al., 2010; Herrera et al., 2013) and derived by inverting only single, i.e. ascending or descending, projection. It is worth stressing that the principles and the input data, on which the map of projectable PS – or more generally DInSAR – data is based, are similar to those of the a priori visibility map. However, whereas the latter provides qualitative information by clustering landslide-affected areas according to three visibility classes, the map

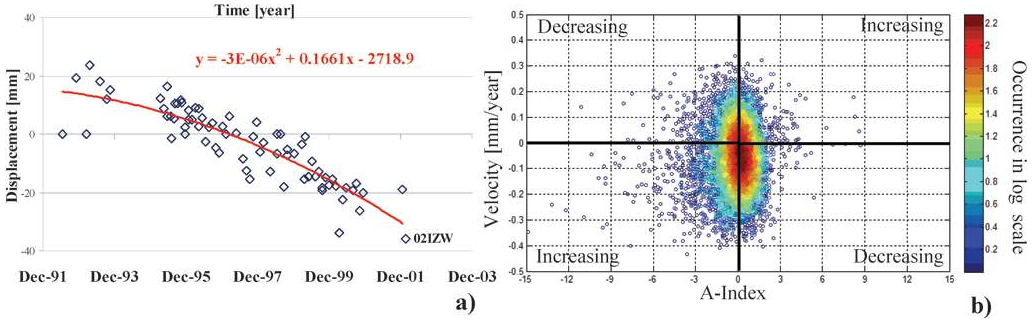

Fig. 7. (a) A-index value represents the coefficient of x squared in the second order polynomial equation fitting the time series; **(b)** A-index vs. LOS-velocity diagram for the ERS ascending (45 images acquired from September 1992–September 2000) PSI data; the colour bar shows the occurrence in log-scale.

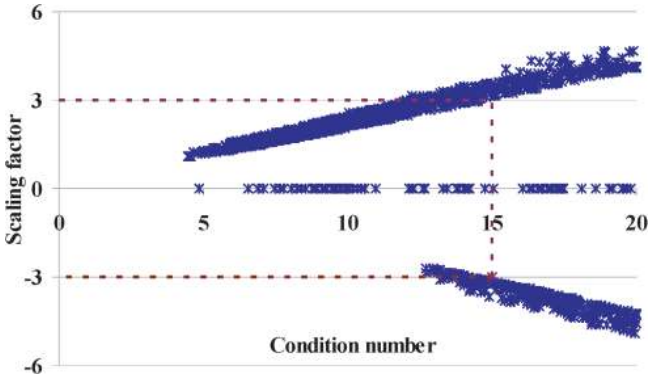

Fig. 8. The condition number vs. the scaling factor of the PS velocity modulus relevant to the ENVISAT ascending dataset (November 2002–July 2010).

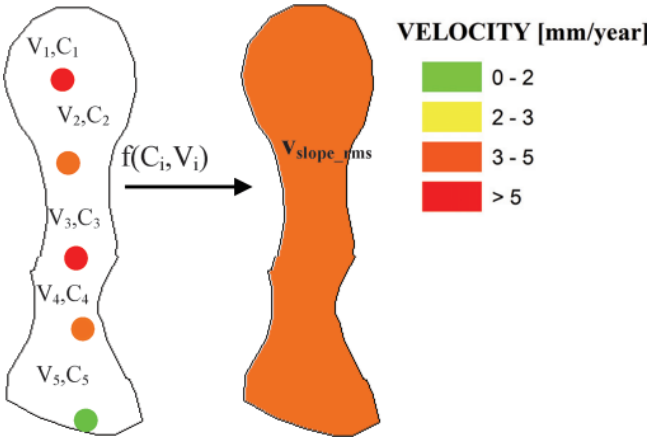

Fig. 9. Example of the landslide velocity computation as a function of both the along-slope velocity (V_{slope}) and the coherence of the PS included in the boundary of the landslide.

of projectable PS data provides a quantitative visibility evaluation of the single PS measured velocity/displacement.

Once the control on the condition number has been carried out, only those PS whose condition number (or scaling factor) is less than 15 (or 3.3) are assumed as "projectable" and, then, used for the following quantitative analyses; the remaining PS are discarded from the following phases and are appointed as "not projectable".

The second phase includes two other operations consisting of the projection of both PS displacement time series and PS LOS velocity along the steepest slope direction, the latter carried out according to the procedures described in Cascini et al. (2010). Subsequently, V_{slope} modulus and the A-Index value relevant to the projected PS time series are computed.

In the third phase, via the joint use of the available landslide inventory map and the information on both V_{slope} and the A-index, each landslide is associated with a velocity value and an increasing/decreasing trend.

The landslide velocity is assumed by some authors (Cigna et al., 2012) as either a simple average on PS velocity values within each landslide or as the maximum recorded value. In this work only those landslides exhibiting a minimum density of about 20 projectable PS km^{-2} or at least 3 projectable PS (Meisina et al., 2008; Notti et al., 2010) are considered in order to discard displacements more likely associated with single targets (e.g. single building structural settlements, etc.) rather than to landslides. Then the landslide velocity (Fig. 9) is computed as the root mean square PS velocity along the slope according to the equation:

$$V_{\text{slope\_rms}} = \left(\frac{\sum_{i=1}^{N} w_{ci}\, V_{\text{slope\_i}}^2}{\sum_{i=1}^{N} w_{ci}} \right)^{1/2} = \left(\sum_{i=1}^{N} \frac{w_{ci}}{w_{cN}} V_{\text{slope\_i}}^2 \right)^{1/2}$$

$$w_{ci} = \frac{(1-\varepsilon_{\min})}{(C_{\max} - C_{\min})}(C_i - C_{\min}) + \varepsilon_{\min}, \qquad (1)$$

in which weight values are established on the basis of the PS coherence (i.e. the higher the PS coherence, the higher the weight value).

In Eq. (1): i refers to the ith PS within the boundary of the landslide; N is the total number of PS within the boundary of

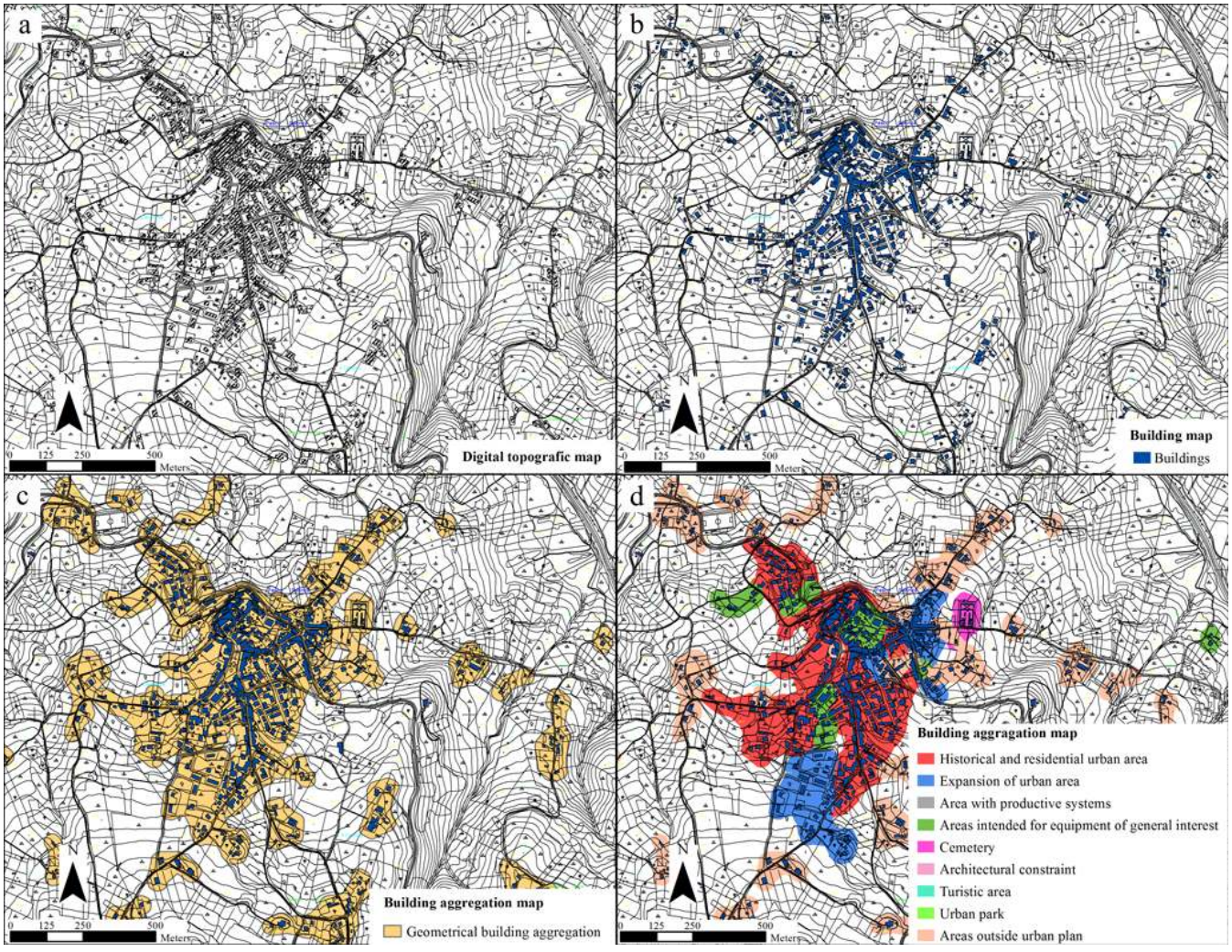

Fig. 10. **(a)** The urban centre of Pesco Sannita municipality; **(b)** identification of buildings; **(c)** definition of building aggregations only on geometrical bases; **(d)** building aggregations distinguished according to the occupancy type.

the landslide; w_{ci} is the coherence weight of the ith PS within the landslide boundary; w_{cN} is the sum of w_{ci}; $V_{\text{slope\_i}}$ is the velocity along the slope of ith PS; $C_{\max}$ is the maximum coherence value of the used dataset; $C_{\min}$ is the minimum coherence value of the used dataset; C_i is the coherence value of the ith PS within the boundary of the landslide; $\varepsilon_{\min}$ is a positive number not greater than 1 defining the weight of the PS with the smallest coherence. In the analyses, $\varepsilon_{\min}$ value was fixed equal to 0.2 thus assigning a weight of 20 % to the smallest coherence value.

The trend of each single covered landslide is conservatively assumed as increasing if at least 30 % of the PS found within the landslide boundary exhibit "increasing" time series.

In the fourth phase, differently from other proposals recoverable in the scientific literature (Cigna et al., 2012; Bianchini et al., 2012; Righini et al., 2012), the velocity threshold is set for a given landslide taking into account the inaccuracy of DInSAR measurements and the scaling factor pertaining to the landslide (derived as root mean square of the scaling factor of the PS in the landslide) as it is described in detail in the Appendix. Subsequently, the mapped landslides are distinguished as "moving" (if their velocity exceeds the threshold), "not moving" (if their velocity is lower than the threshold) or "no data" (if less than 20 projectable PS km^{-2} or less than 3 projectable PS are found within the landslide boundary).

The information achieved in the fourth phase is ready to be merged with the results of damage survey data analysis via the matrix described in Sect. 4.3.

4.2 The procedure for the analysis of damage data

In order to use the damage dataset for a joint analysis with DInSAR data, facilities (buildings and roads) interacting with landslide affected areas must be identified (Cascini et

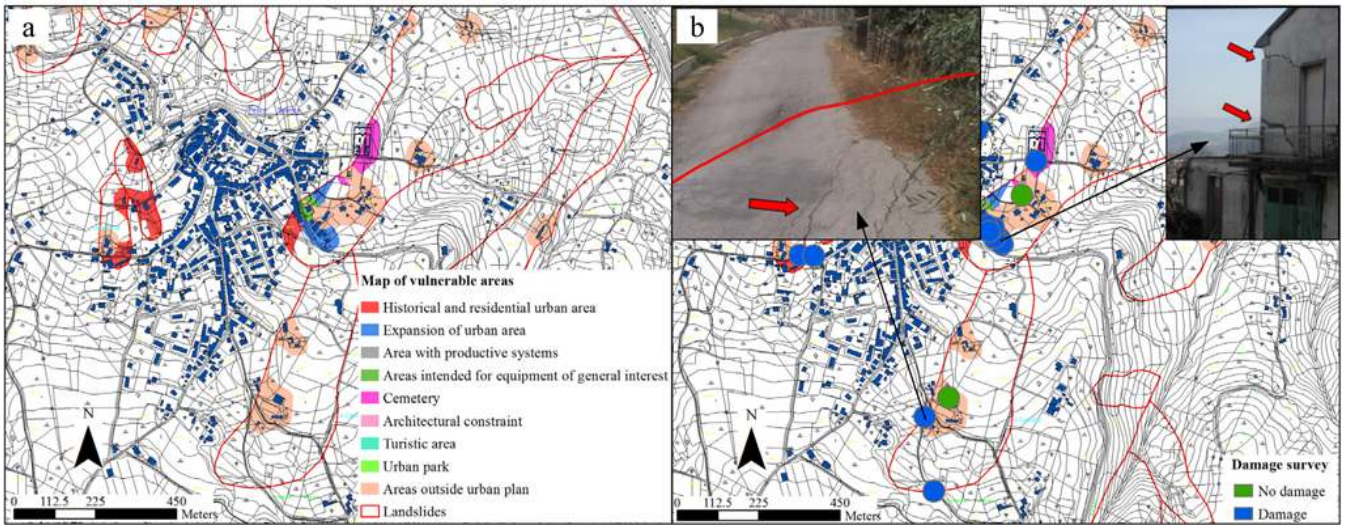

Fig. 11. (a) Vulnerable areas; **(b)** vulnerable areas and roads with damage or no damage. Examples of damages to one road (differential settlements and cracks on the road pavement), induced by an active earth flow, and to one masonry building (significant cracks in the elements of the structure) induced by an active rotational slide-earth flow.

al., 2008; Pisciotta, 2008). To this aim, with reference to a given municipal territory of the study area (Fig. 10a), the existing buildings are firstly identified (Fig. 10b) on the basis of the available digital topographic map at large scale (1 : 5000); then, homogeneous building aggregations are defined considering that, at medium scale, the identification of a single building (van Westen, 2004) is impracticable and not significant.

In particular, building aggregations (Fig. 10c) are sketched as planar figures whose geometry is convex outwards and, therefore, do not present any cusps on their perimeters. Around each structure, a buffer of 25 m is considered in order to take into account the graphical error related to the working scale (1 : 25 000) as well as the possibility to have additional constructions in the property; moreover, the maximum allowable distance between two buildings is assumed lower than 100 m so that urbanised zones prevail on non-urbanised areas within each unit (Ferlisi and Pisciotta, 2007; Cascini et al., 2008). Finally, building aggregations are further distinguished as homogeneous units – in terms of occupancy type – thanks to the information gathered from the available urban plans (Fig. 10d).

The intersection of the obtained building aggregations with the landslide inventory map allows the identification of the so-called "vulnerable areas" (Fig. 11a). These latter, in turn, are classified as vulnerable areas with or without damage whether at least one damaged building within their perimeter is recorded (Fig. 11b).

The roads are considered as single damaged or not damaged elements according to the information provided by the damage surveys (Fig. 11b).

4.3 DInSAR–Damage data matrix

The matrix-based approach was already tested in the scientific literature concerning the use of PSI data for the evaluation of the landslide state of activity (MATTM, 2010; Cigna et al., 2012; Bianchini et al., 2012; Righini et al., 2012). This work adopts a new matrix whose innovation relies on the introduction of data concerning survey-recorded damage to facilities as indicators of movement, in addition to PSI (or more generally DInSAR) data and available landslide inventory maps. In particular, once the two datasets (i.e. DInSAR and facility damage data) have been separately analysed, the DInSAR-Damage matrix is applied to those landslides for which DInSAR datasets, referred to different time periods (e.g. ERS and ENVISAT), are available.

As shown in Fig. 12, the input data to the matrix are the state of activity (i.e. active or dormant) provided by the landslide inventory map; the information gathered from the damage survey (i.e. landslide with damage, landslide with no damage, landslide with no damage survey); the condition of movement derived from ERS DInSAR data (i.e. moving or not moving landslide). Of course, with reference to the latter information, only the landslides for which the velocity can be computed (Sect. 4.1) are considered. The above data are then cross-checked with the evidence of movement derived from ENVISAT DInSAR data, which represent the updated information since ERS data, landslide inventory map and damage survey data refer, respectively, to periods 1992–2000, 2001, 2000; whereas ENVISAT data refer to a following period of time (2003–2010). The increasing/decreasing trend (Sect. 4.1) exhibited by a given landslide according to ERS data (displacement time series and velocity) represents additional information, which is used when ERS and ENVISAT

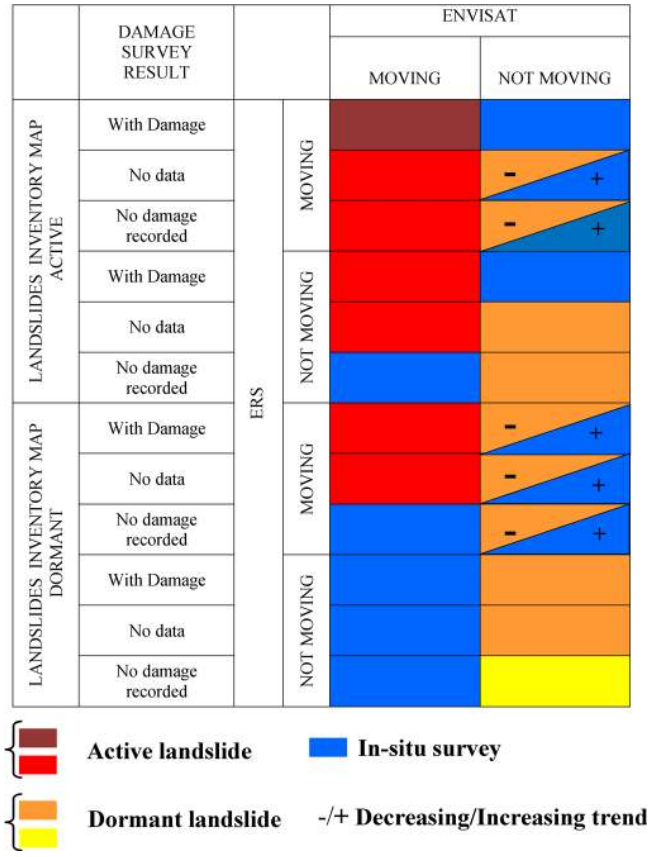

Fig. 12. The DInSAR-Damage matrix.

data provide different movement conditions of the landslide in order to support the definition of the updated state of activity. According to the landslide inventory map of NBA LGV territory (Sect. 2), the updated state of activity can be distinguished between active or dormant; moreover, in situ surveys are recommended when the available information is not sufficient to assign the new state of activity. In two cases the state of activity can be more confidently assumed as active (dark red cell in Fig. 12) or dormant (light yellow cell in Fig. 12) corresponding to the concordant combination of all available indicators: active mapped landslide with damage and both ERS and ENVISAT moving evidences, for the former case; dormant mapped landslide with no damage recorded and both ERS and ENVISAT not moving evidences, for the latter case. In the other cases the state of activity derives from the information provided by the majority of the indicators (mapped landslide activity, damage, ERS and ENVISAT data) giving more weight to the most recent data (ENVISAT data). As for the cells divided in two triangles (Fig.12), the state of activity is determined using the additional information provided by the sign of the trend (i.e. increasing +; decreasing –). For instance, once all the other indicators were taken into account, if for an ERS moving landslide the assumed trend is decreasing and for ENVISAT the landslide is not moving it can be argued that during the ERS period (1992–2000) the landslide was decelerating and it stopped during the ENVISAT period (2003–2010); thus, the current state of activity can be set to dormant. On the contrary, if for an ERS moving landslide the assumed trend is increasing and according to ENVISAT the landslide is not moving, it can be inferred that the landslide was accelerating during 1992–2000 and it stopped during 2003–2010, thus the current state of activity cannot be easily defined and in situ investigations are necessary.

5 Analysis at medium scale (1 : 25 000)

5.1 DInSAR data

With reference to the study area, the a priori landslide visibility map was firstly generated according to the adopted methodological approach (Fig. 6). The obtained map (Fig. 13a and b) highlights that the areas visible with difficulty on both orbits – namely slopes facing north or south (Cascini et al., 2009) – correspond to 23.6 % of the total landslide affected areas; the visible areas on ascending orbit (Fig. 13b) correspond to 33.5 %; whereas on descending orbit (Fig. 13a) the percentage raises up to 42.8 %. This is confirmed by the higher number of PS on descending orbit datasets (5024 PS of which 60 % in visible areas, 25 % in areas visible with difficulty and 15 % in not visible areas) than on ascending orbit datasets (4882 PS of which 53 % in visible areas, 25 % in areas visible with difficulty and 22 % in not visible areas) which are found within landslide affected areas. Moreover, the percentage of PS-covered (by at least 3 PS or with more than 20 PS km^{-2}) landslides is equal to 16 % for ERS sensor and 20 % for ENVISAT. In this first phase of activities the A-Index was also computed for each available PS of the ERS dataset.

Through the map of projectable PS (Fig. 14a and b) the available PS were distinguished as projectable and not projectable depending on the value of the scaling factor (lower or higher than 3.3). In particular, around 53 % out of the total ERS-PS (Fig. 14a) and 47 % of the ENVISAT-PS (Fig. 14b) resulted projectable.

Focusing on the projectable PS, firstly the V_{slope} value was calculated for each PS; after that, the landslide velocity was computed for each covered phenomenon according to ERS (Fig. 15a) and ENVISAT (Fig. 15b) data. The achieved results, grouped for the different landslide types (i.e. earth flows, rotational slides and rotational slide-earth flows), show that the computed landslide velocities attain comparable values not exceeding a limit of 25 mm yr^{-1} (Fig. 15c) that is slightly over the velocity value of 16 mm yr^{-1} discriminating extremely slow against very slow phenomena (Cruden and Varnes, 1996). With respect to creep phenomena, earthflow creeps and deep-seated gravitational movements, the computed velocity values do not exceed 7 mm yr^{-1}, thus falling

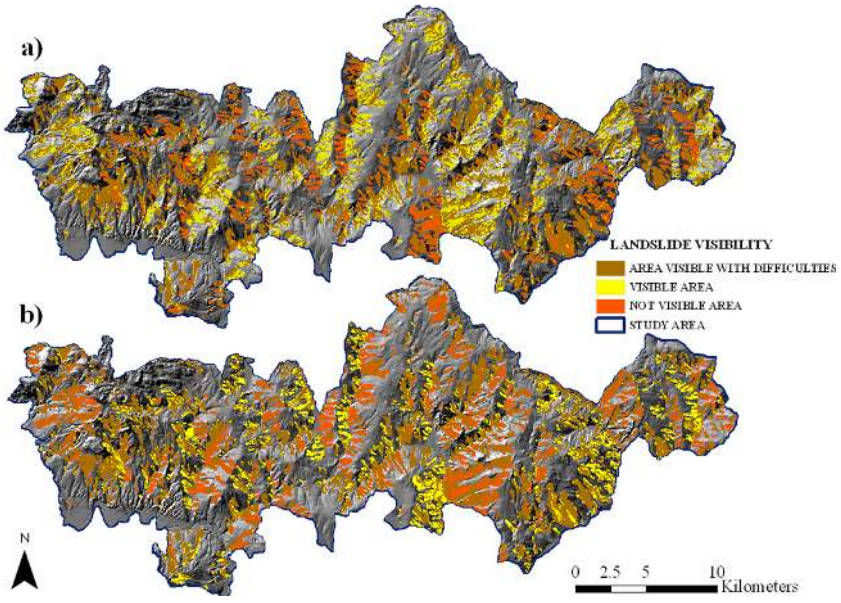

Fig. 13. The a priori landslide visibility map for the study area on descending **(a)** and ascending **(b)** orbit.

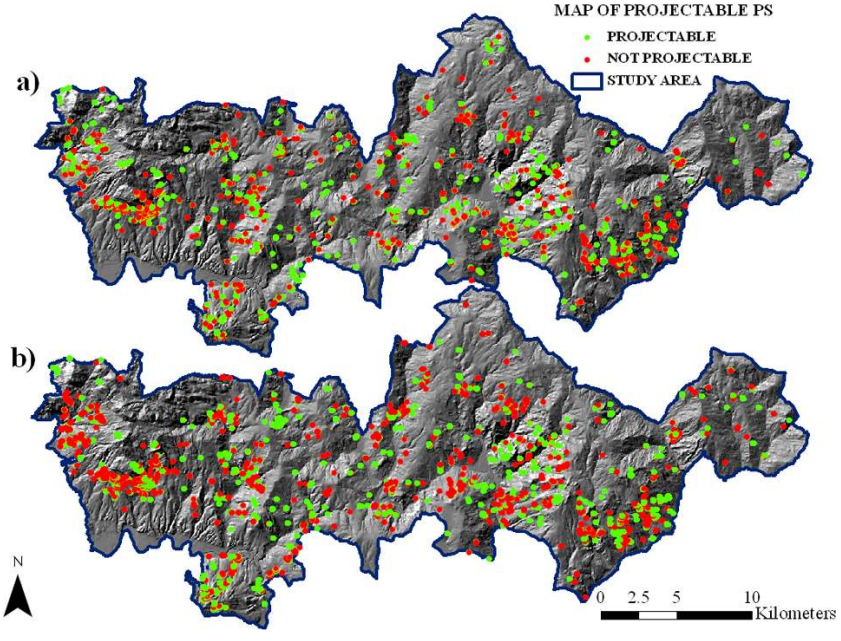

Fig. 14. The map of projectable PS for ERS **(a)** and ENVISAT **(b)** datasets.

within the range of extremely slow phenomena (Cruden and Varnes, 1996). However, as already pointed out by Cascini et al. (2010) the computed landslide velocities refer to values averaged in time (period of observation of PSI dataset) and in space (amongst the velocities of the PS included in the boundary of the same landslide), whereas Cruden and Varnes (1996) reasonably refer to the maximum velocity value attained by a given – superficial or internal – point of a landslide displaced mass during its paroxysmal phase of movement.

The landslide velocity maps (Fig. 15a and b) are preparatory to the generation of the map in Fig. 16 where PS-covered landslides are appointed as moving, not moving or no data according to the corresponding velocity thresholds (see the Appendix). The results highlight that out of a total of 288 landslides covered by projectable ERS data (Fig. 16a) 30 % are moving and 70 % are not moving. With reference to

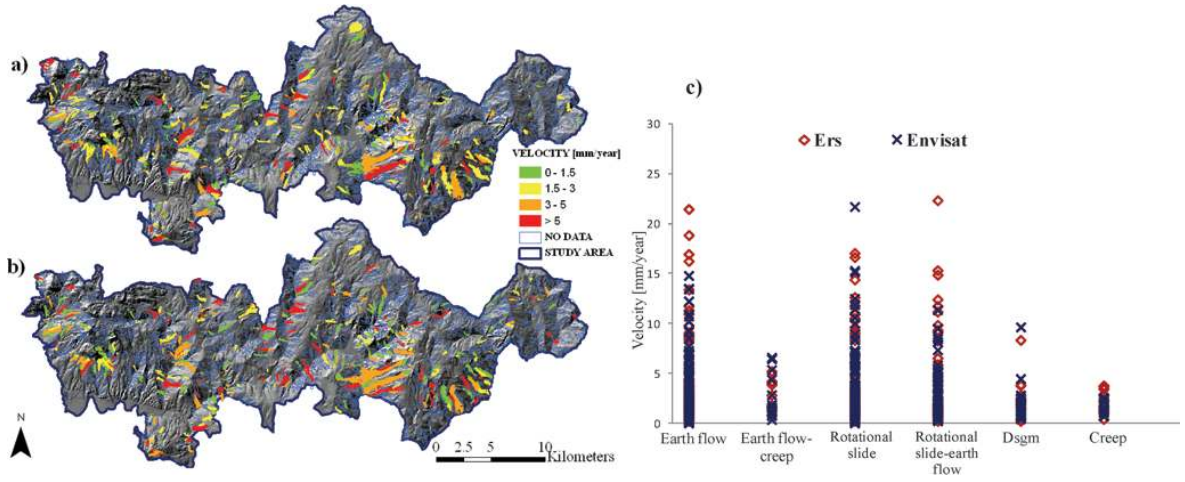

Fig. 15. The PSI landslide velocity map for ERS **(a)** and ENVISAT **(b)** data; **(c)** the computed landslide velocities per different landslide types.

ENVISAT dataset (Fig. 16b) out of 376 landslides covered by projectable ENVISAT data 38 % are moving and 62 % are not moving.

The condition of movement/no movement derived from ERS-PSI data (period 1992–2000) was compared with the state of activity reported in the landslide inventory map (2001) with reference to 249 landslides (53 active and 196 dormant) classified as earth flows, rotational slides or rotational slide-earth flows. In Fig. 16c it can be noticed that over 53 active landslides 36 % are moving according to ERS landslide velocities; whereas 89 % of 196 dormant phenomena are not moving.

Finally, an increasing/decreasing trend was assumed for each landslide according to the previously described procedure (Sect. 4.1) using ERS projected time series.

This latter information together with the abovementioned data plays as input data to the DInSAR-Damage matrix.

5.2 Damage to facilities

With reference to all 21 urbanised municipal territories of the study area and according to the methodology described in Sect. 4.2, the homogeneous aggregations of existing buildings were firstly generated (Fig. 17a). Then, they were intersected with the mapped slow-moving landslide affected areas (Fig. 17b); thus, obtaining the so-called vulnerable areas distinguished on the basis of the buildings' occupancy type (Fig. 17c). On the other hand, the portions of single roads (Fig. 17d) interacting with the inventoried landslides were detected (Fig. 17e and f).

Once identified, vulnerable areas and roads were classified as damaged or not damaged whether at least either one damaged building within their perimeter or damage evidences along the road track interacting with the landslides were recorded. As a result, a total number of 190 vulnerable areas with damage survey (45 % of them damaged and 55 % not damaged) and 228 roads with damage surveys (60 % of them damaged and 40 % not damaged) was recorded.

Then, focusing on landslides interacting with damaged vulnerable areas and/or roads, Fig. 18a shows that – out of a total of 147 inventoried phenomena – 94 (64 %) of them involved only vulnerable roads, 35 (24 %) only vulnerable areas and the remaining 18 (12 %) both vulnerable areas and roads. On the other hand, the landslides interacting with not damaged vulnerable areas and/or roads are 247; these, in turn, can be distinguished among those involving (i) only vulnerable roads (116 corresponding to 47 %), (ii) only vulnerable areas (101 corresponding to 41 %), (iii) both vulnerable areas and roads (30 corresponding to 12 %). Furthermore, Fig. 18b shows that the highest number of slow-moving landslides interacting with damaged vulnerable areas and/or roads pertains to the earth flow type, immediately followed by rotational slide type.

The distribution of the above described results over the study area is shown in Fig. 19a and b where a comparison among the state of activity defined in landslide inventory map and damage survey results with reference to vulnerable areas and/or roads is represented. Over 352 (94 active and 258 dormant) landslides – for which the state of activity is reported in the inventory map (i.e. earth flows, rotational slides and rotational slide-earth flows) and detailed damage surveys are available – a good agreement is attained between dormant landslides and not damaged vulnerable areas/roads (about 70 %), while the percentage of active landslides on which damages to vulnerable areas/roads were recorded is around 51 %.

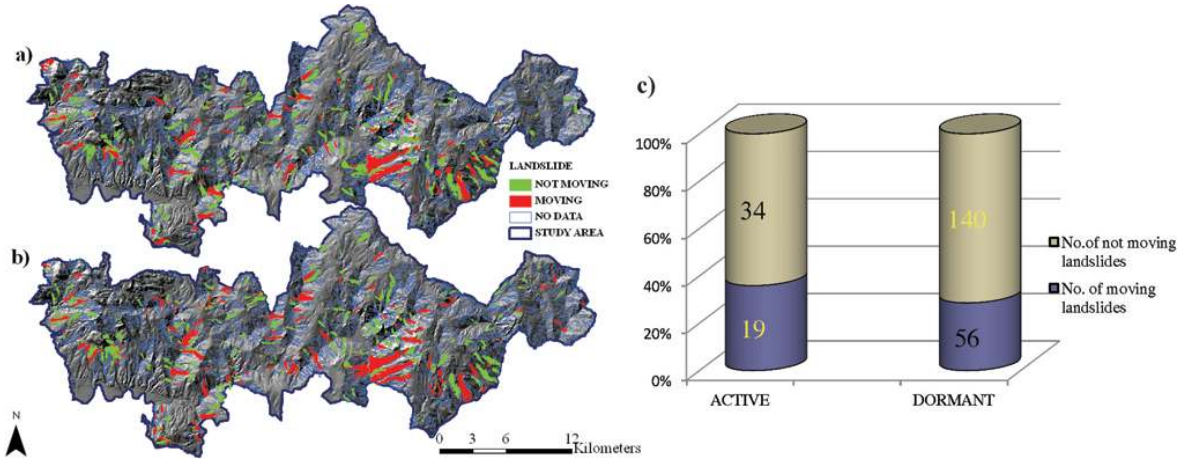

Fig. 16. Map of moving/not moving landslide according to both ERS **(a)** and ENVISAT PSI **(b)** data; **(c)** comparison among the state of activity derived from either the landslide inventory map or the indication of movement derived from ERS-PSI data.

5.3 Joint analysis of DInSAR and damage to facilities datasets

PSI-derived evidences of movement and the results of damage survey dataset were compared showing that over 44 PSI-moving landslides, for which damage survey results are available, 57 % of surveyed facilities recorded damage; whereas for landslides appointed as not moving (85), 58 % of the total did not exhibit damage during surveys (Fig. 20). This may be related to the constraints arising from the adopted scale of work. Indeed, at medium scale (1 : 25 000), the role played by some relevant factors (Sect. 3.2) in influencing the damageability of facilities interacting with slow-moving landslide bodies cannot be clearly highlighted, e.g. the relative position of facilities within the landslide affected areas. In the study area, nine not damaged building aggregations interacting with ERS-PSI moving earth flows were found to be in the middle portion of the landslide, usually affected by translational movements (Cascini et al., 2010). Therefore, the involved buildings may have not suffered damages because foundations were mainly subjected to absolute (not differential) displacements which can be tolerated by the superstructures.

6 Updating of landslide inventory maps

6.1 The state of activity

The DInSAR-Damage matrix was applied to update the state of activity of 167 landslides (29 active and 138 dormant, see Fig. 21a), for which both ERS and ENVISAT-PSInSAR data are available. As a result, 33 active and 83 dormant landslides are distinguished (Fig. 21b) and for 51 landslides further in situ surveys are necessary since the available information is not enough to define the state of activity (Fig. 21b).

A cross-check with the available pre-existing landslide inventory map (Fig. 21a) reveals that 91 landslides confirm their previous state of activity, whereas for 25 it changes. In particular, 19 landslides pass from dormant to active and 6 from active to dormant.

A field validation test of the outcomes of the DInSAR-Damage matrix over such an extended area was carried out by randomly selecting 10 % out of the total number of active and dormant landslides whose state of activity was either confirmed or changed with respect to the available landslide inventory. In 2012, field surveys were carried out on these areas to detect evidences of movement in structures and infrastructures. These surveys highlighted that, over 19 investigated landslides, the matrix-based state of activity was confirmed for 15 of them, being not confirmed for the remaining 4 landslides. Some examples are reported hereafter.

The first example refers to a rotational slide-earth flow located in the municipality of Pesco Sannita in Benevento Province (Fig. 22a–g). This landslide (Fig. 22a) reported as active on the landslide inventory map showed a velocity around 8 mm yr^{-1} (Fig. 22b) from the analysis of PSI-ERS data. As for the damage, the survey carried out in 2000 (Fig. 22d) recorded the presence of significant cracks in the elements of one masonry building (on the right in Fig. 22d) and the tilting of another masonry building (on the left in Fig. 22d), whose stability and serviceability were seriously affected, both located in the head of the landslide body (Fig. 22a). The availability of ENVISAT-PSI dataset allowed to classify the landslide as moving – with a computed velocity of 5 mm yr^{-1} (Fig. 22c) – and according to the DInSAR-Damage matrix the assumed state of activity was confirmed as active (dark red in the matrix, first cell of the first column). To check the reliability of this assumption two damage surveys were performed, as it is shown in Fig. 22e–g, in 2006 and 2012 both showing the presence of cracks on the building

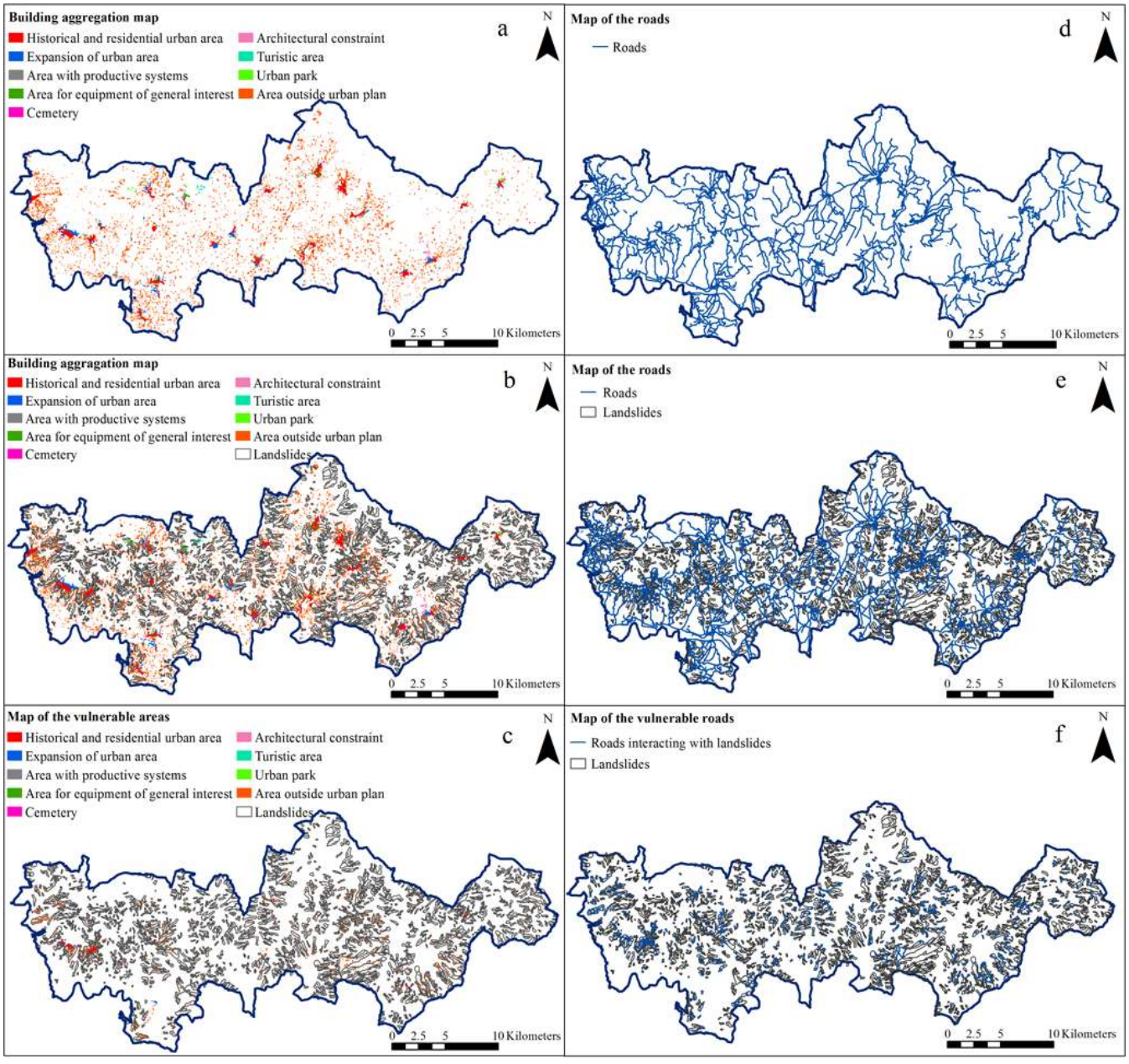

Fig. 17. **(a)** Building aggregation map; **(b)** map of building aggregations and landslides; **(c)** map of vulnerable areas; **(d)** map of the roads; **(e)** map of the roads and landslides; **(f)** map of the vulnerable roads.

on the right. Moreover, during the survey of 2012 the building on the left resulted to have been demolished.

A second example is shown in Fig. 23a–h with reference to an earth flow (Fig. 23a), in the municipal territory of Reino (Benevento Province), reported as dormant in the landslide inventory. According to the analysis of both ERS and ENVISAT computed velocities (respectively equal to 9.8 mm yr^{-1} and to 5 mm yr^{-1}) (Fig. 23b) the landslide resulted as moving. Moreover, during the damage survey carried out in year 2000 (Fig. 23c–e) cracks were recorded on masonry row houses located along the boundary of the landslide body. The implementation of the DInSAR-Damage matrix allowed the classification of this landslide as active (seventh cell of the first column, Fig. 12). To validate this assumption, the results of a damage survey carried out in 2012 were used (Fig. 23f–h). In particular, Fig. 23f shows a wall where the width of the vertical cracks recorded in year 2000 (Fig. 23c) increased (Fig. 23f) as well as the occurrence of some inclined cracks (Fig. 23h) on a wall which during the previous survey did not exhibit any cracks (Fig. 23e).

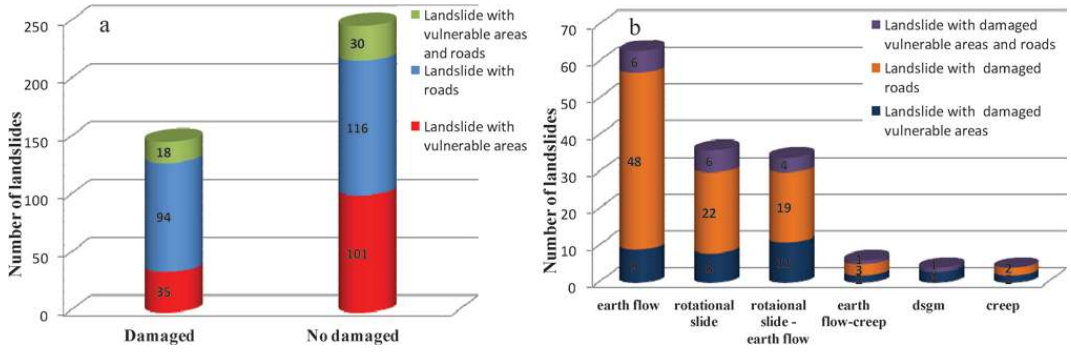

Fig. 18. (a) Number of landslides with or without damaged vulnerable areas and/or roads; **(b)** number of landslides with damaged vulnerable areas and/or roads distinguished according to the type.

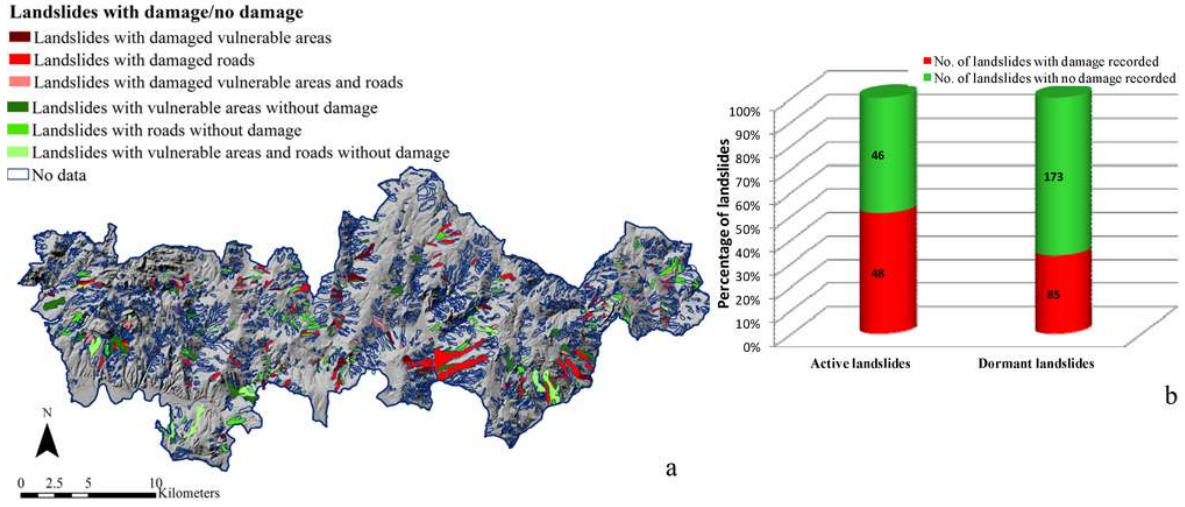

Fig. 19. (a) Map of landslides with or without recorded damage to vulnerable areas and/or roads; **(b)** comparison among the state of activity of landslides derived from the inventory map and the results of damage surveys.

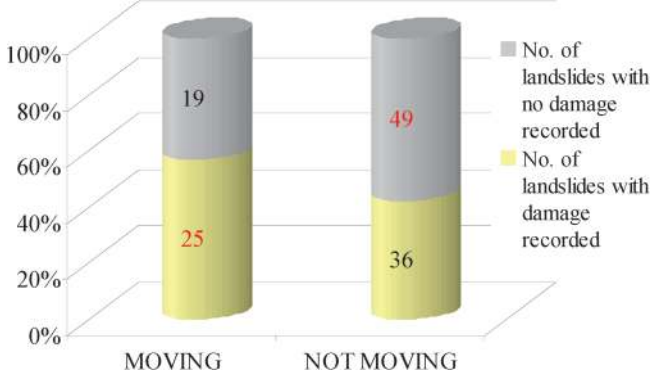

Fig. 20. Comparison among PS-derived evidence of movement on landslides and the results of damage survey.

Moreover, with reference to the same group of structures during the survey dated 2012 some cracks on recently restored building façades were recorded.

The last example in Fig. 24a–h concerns a dormant rotational slide located in the municipality of San Giorgio la Molara (Benevento Province). In particular, Fig. 24a shows that the head of the landslide involves some buildings and the ERS velocity vectors exhibit mostly (5 out of 6 PS) decreasing trends. The computation of the ERS landslide velocity (3.6 mm year^{-1}) exceeding the ERS velocity threshold (3.4 mm yr^{-1}) (Fig. 24b) allows defining the landslide as moving and, according to the majority of PS-derived trends, a decreasing trend is associated with the landslide. The analysis of ENVISAT data (Fig. 24c–d) highlights that the landslide is not moving since the landslide velocity (0.9 mm yr^{-1}) is lower than the computed velocity threshold (3.8 mm yr^{-1}). For this landslide no damage survey data is available so entering the DInSAR-Damage matrix (eighth cell of the second column) and considering the ERS decreasing trend (sign –) the state of activity should be set to dormant. This result was validated by a damage survey carried out in 2012 showing that the buildings located in the head of the rotational slide

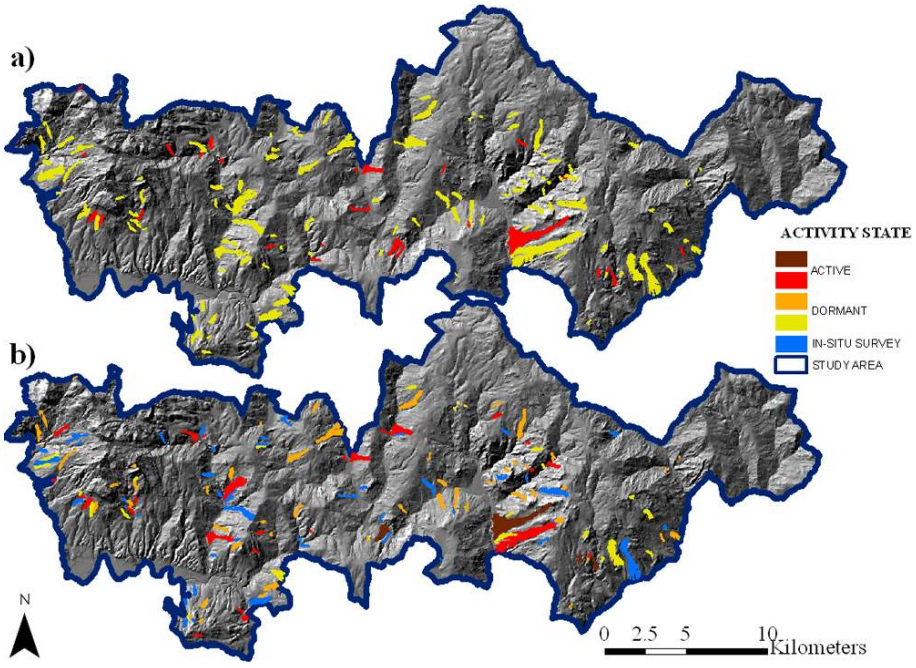

Fig. 21. Results of the application of the DInSAR-Damage matrix: the pre-existing **(a)** and the updated **(b)** landslide state of activity.

(Fig. 24e–h), mainly consisting of reinforced concrete structures, did not exhibited any cracks or damages.

6.2 Detection of unmapped phenomena

The automated detection and mapping of slow-moving landslide phenomena via remote sensing techniques (radar and optical) over wide areas is a challenging topic. In the present study the availability of the geomorphological map (1 : 25 000 scale) of the NBA LGV suggested to focus the analyses on the portions of the study area mapped as hollows. As described in Cascini et al. (2009) these areas are characterized by geomorphological settings similar to landslide affected areas; therefore, they can be preliminarily analysed prior to proceeding to the updating of a given inventory map. In the study area over a total of 1580 hollows 189 resulted covered by projectable ERS-PSI data. Focusing on the hollows covered by at least three PS or with a density higher than 20 PS km^{-2}, the velocities were computed and 33 hollows resulted moving (Fig. 25a). For eight of these hollows the damage survey results dated 2000 were available and within the boundaries of three of them damages to facilities were recorded.

A similar comparison was then carried out with ENVISAT-PSI data whose information covered 233 hollows, 40 of which resulted as moving (Fig. 25b).

One of these is reported in Fig. 26a–g which show a moving hollow (in red in Fig. 26a) located at the head of a rotational slide earth flow (in gray in Fig. 26a) in the municipality of Campolattaro (Benevento Province). The computed velocity (1.7 mm yr^{-1}) for ERS data (Fig. 26b) approaches the movement threshold (2 mm yr^{-1}), whereas for ENVISAT data the threshold (2.8 mm yr^{-1}) is exceeded by the hollow velocity value (4.8 mm yr^{-1}) with some PS velocity reaching up to about 10 mm yr^{-1}. In this area damage surveys were also carried out. The results of both the surveys in 2000 (Fig. 26c–d) and 2012 (Fig. 26e–g) show the tilting of a masonry building whose serviceability is definitively compromised. Moreover, the vertical crack pattern recorded in correspondence of the joint between the building and its entry structure (Fig. 26f and g) exhibits an overall increase during the period 2000–2012. These evidences could be related to either the activation of a landslide phenomenon or to a retrogressive movement starting from the head of the rotational slide located downslope.

7 Discussion and conclusion

The updating of slow-moving landslide inventory maps is a timely issue which can turn out to be an extremely expensive and time consuming task if carried out with traditional techniques. Remote sensing data represent a valuable tool in such activities, although shared standardized procedures are still lacking and the potential of this kind of data has not been fully exploited.

In the present paper PSI data, combined with geomorphological, topographic and optical data in order to detect/map/monitor slow-moving landslides, were jointly analysed with the results of damage surveys to structure/infrastructures recorded within landslide affected areas.

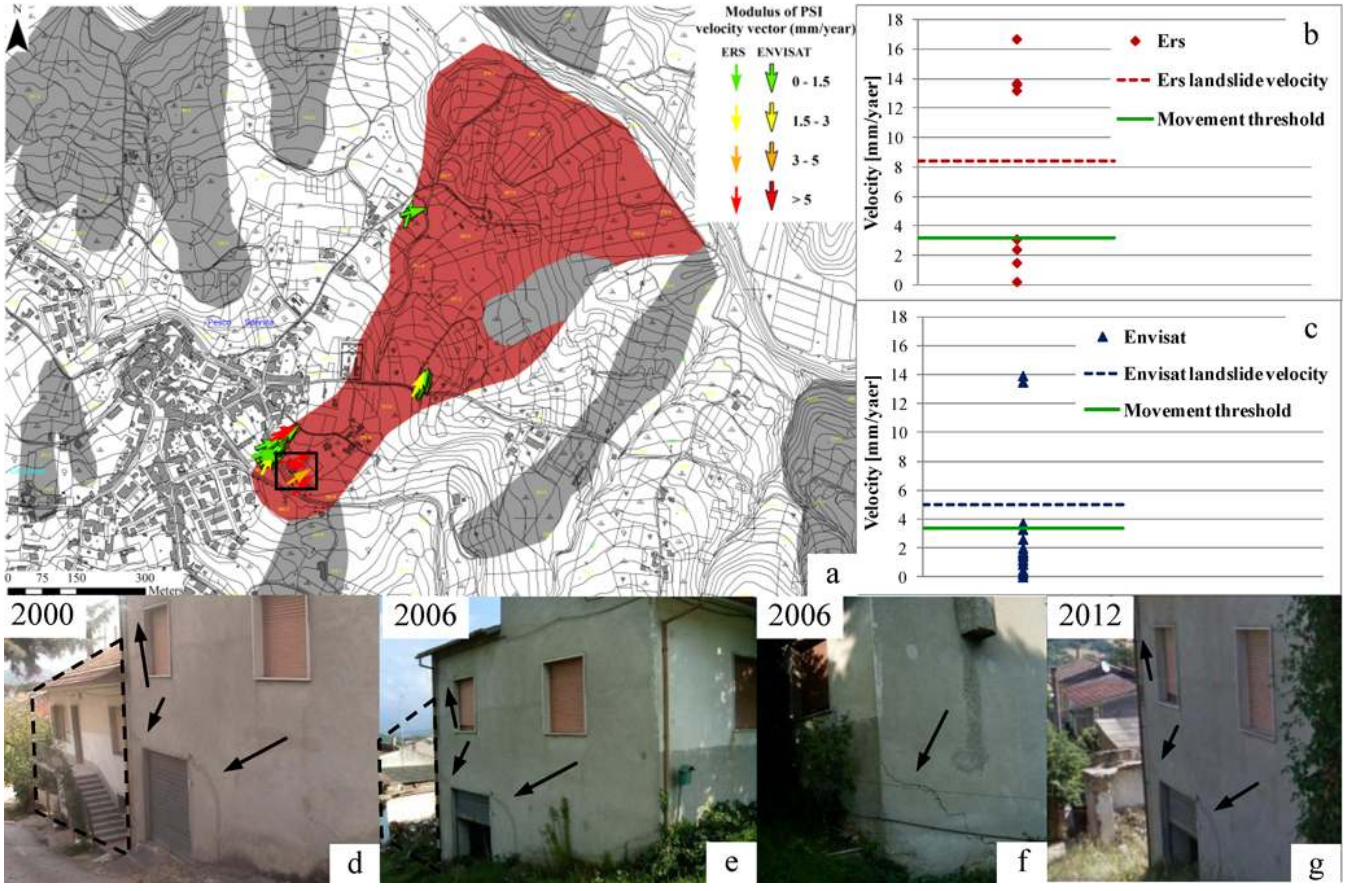

Fig. 22. An active rotational slide-earth flow in the municipality of Pesco Sannita (Benevento Province): **(a)** the inventory map with ERS/ENVISAT PS velocity vectors; **(b–c)** diagrams of the ERS/ENVISAT velocity values for the PS located within the landslide boundaries and indication of both the computed landslide velocity and the computed movement threshold; **(d–g)** photos of two buildings located in the head of the landslide with highlight on the damage recorded during the survey dated 2000, 2006, 2012.

The adopted scale of analysis (1 : 25 000) corresponds to that of the available landslide inventory map. This scale called for some necessary pre-processing of both PSI and damage data prior to merging them into the DInSAR-Damage matrix due to their point-wise characteristic.

In agreement with the approaches currently adopted in the scientific literature, a landslide velocity value for each covered landslide was defined. This operation was performed introducing a quality control of PSI data; in particular, after selecting the most reliable PS and projecting their velocity along the steepest slope direction, the velocity weighted on the coherence values of the PS falling within the boundary of a given landslide was computed for each landslide. A variable landslide velocity threshold, which takes into account both V_{LOS} inaccuracies and V_{LOS}–V_{slope} scaling factor values, was then fixed for each landslide and compared with the computed velocity in order to distinguish among moving or not moving landslides.

The scale of analysis required the generation of the map of building aggregations and roads whose intersection with landslide affected areas allowed the identification of the vulnerable areas.

By separately comparing the state of activity reported in the landslide inventory map with PSI or damage-derived information an overall similar agreement between the active (51 %)/dormant (70 %) (from the inventory) or moving (57 %)/not moving (58 %) (from DInSAR) phenomena with damage occurrence was highlighted. The matching percentages, although not exceeding 70 %, encourage further deepening of this kind of analysis since the use of DInSAR data and damage surveys over wide areas can be less expensive than extensive field surveys. The current limits to the application of the described methodology are mainly related to the availability of PSI data on landslides (depending on vegetation, aspect, slope, the projected velocity value); the availability of thematic maps (geomorphological map, landslide inventory map) and damage survey results. Therefore, the number of landslides whose state of activity can be updated can turn out to be limited. In this regard, it is worth stressing that future improvements concerning both ground

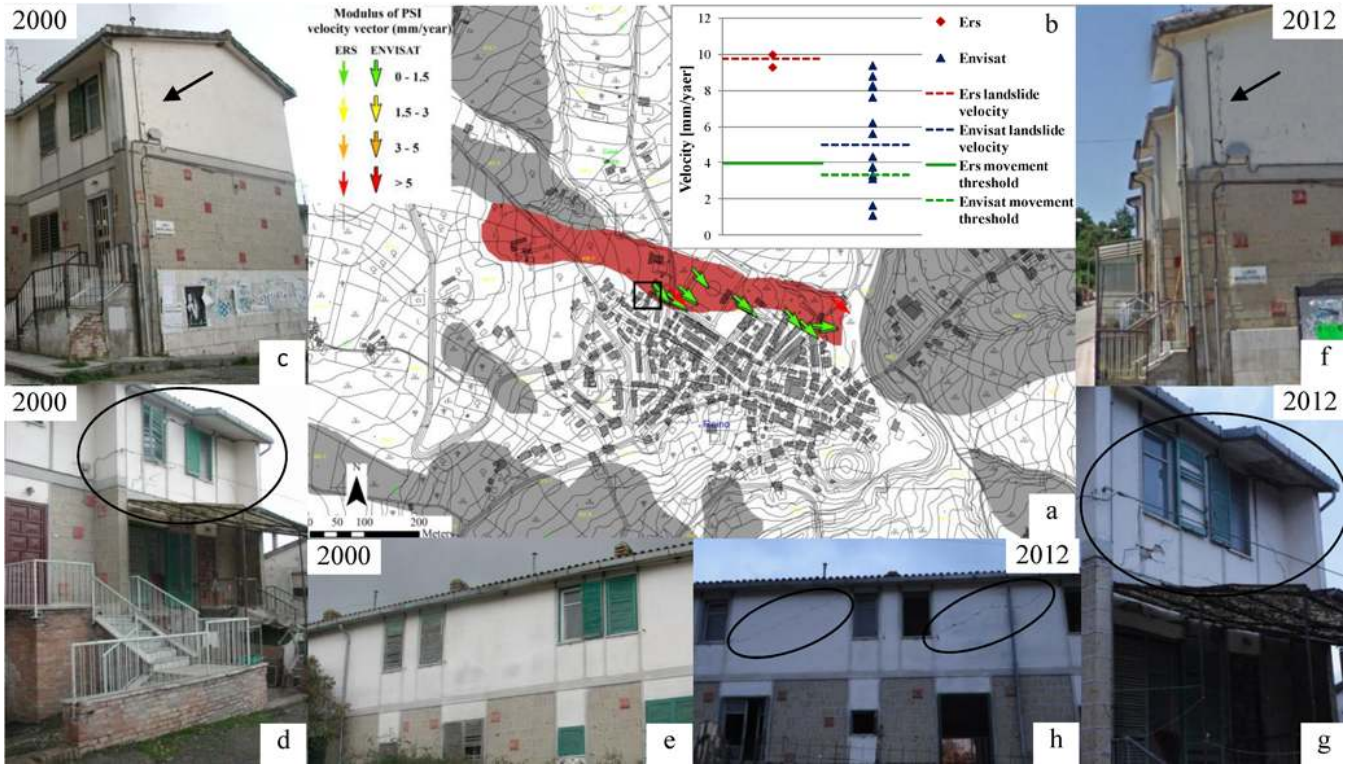

Fig. 23. A dormant earth flow in the municipality of Reino (Benevento Province): **(a)** the inventory map with ERS/ENVISAT PS velocity vectors; **(b)** diagrams of the ERS/ENVISAT velocity values for the PS located within the landslide boundaries and indication of both the computed landslide velocity and the computed movement threshold; three different views of row-houses located on the middle boundary of the landslide (see the black square in **a**) with highlight on the damage recorded in the surveys dated 2000 **(c–e)** and 2012 **(f–h)**.

resolution and reduced revisiting time will allow an increased DInSAR coverage over landslide affected areas. In addition, preliminary damage surveys carried out for the purpose of analyses at 1 : 25 000 scale could also benefit from the use of high resolution optical sensors, thus significantly reducing the number of facilities to be investigated.

As for the updating of the inventory map the aforementioned enhancements could result in fostering the use of the DInSAR-Damage matrix since they will widen the sample of the landslides to which it can be applied. The validation tests of the matrix carried out up to now, although still limited due the extension of the study area, encourage future tests to better enquire about the reliability of the results. Moreover, the use of the matrix seems helpful in planning more expensive conventional surveys only with reference to around 30 % of the analysed phenomena (i.e. those appointed as "in situ surveys required").

Finally, the procedure adopted for the detection of unmapped phenomena tried to take advantage of the information contained in the available geomorphological map using remote sensing data. As a result, several areas which are likely to be affected by landslide phenomena were selected. In this regard, a further step will deal with the joint application of Object-Based Image Analysis techniques which are currently considered as the most promising ones for the digital recognition of landslides especially when thematic maps are not available.

Appendix A

This appendix is devoted to explaining the adopted method to establish if a given slow-moving landslide can be defined as moving. In particular, this method is based on the analysis of V_{slope} values pertaining to the projectable PS located within the landslide boundaries, taking account of both PS V_{LOS} inaccuracies and the scaling factor values from V_{LOS} to V_{slope}.

First of all it must be observed that a landslide is usually defined as moving when the velocity of its body (or of a part of it) is greater than zero. In order to verify the attainment of this condition on the basis of PSI-derived velocities, it must be considered that these values are characterized by inherent inaccuracies. As a consequence, the condition of landslide movement should imply the exceedance of a PS velocity threshold which takes into account the abovementioned inaccuracies.

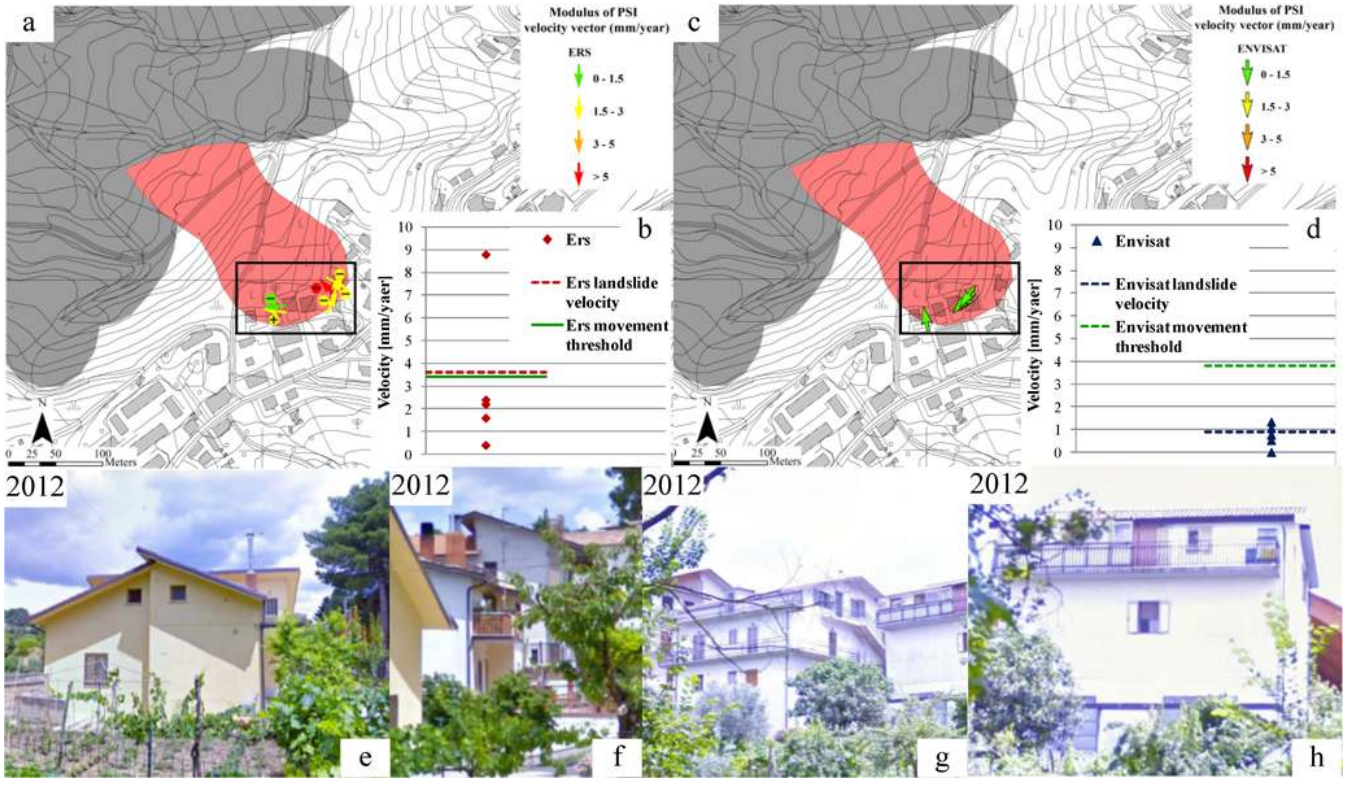

Fig. 24. A dormant rotational slide in the municipality of San Giorgio La Molara (Benevento Province): **(a)** the inventory map with ERS PS velocity vectors and indication of the increasing (+) or decreasing (–) trend of the displacement time series; **(b)** diagrams of the ERS velocity values for the PS located within the landslide boundaries and indication of both the computed landslide velocity and the computed landslide movement threshold; **(c)** the inventory map with ENVISAT PS velocity vectors; **(d)** diagrams of the ENVISAT velocity values for the PS located within the landslide boundaries and indication of both the computed landslide velocity and the landslide movement threshold; **(e, f, g, h)** different views of buildings located in the head of the landslide referring to the survey carried out in 2012.

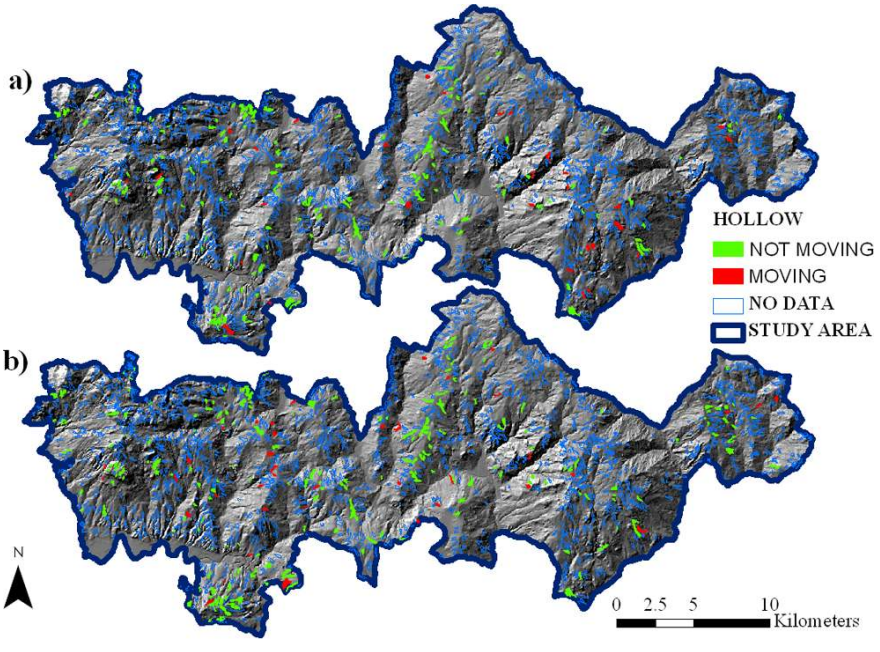

Fig. 25. Map of the hollows in the study area distinguished according to ERS **(a)** and ENVISAT **(b)** PSI data analysis.

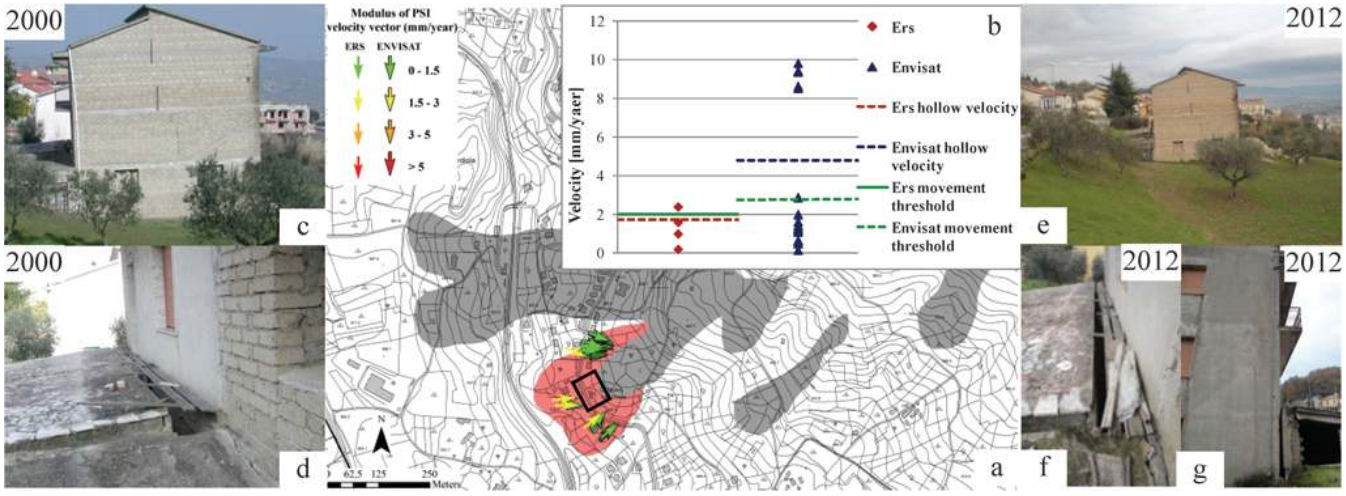

Fig. 26. A hollow located in the municipality of Campolattaro (Benevento Province): **(a)** map the hollow (in red) located at the head of a rotational slide-earth flow (in gray) with ERS/ENVISAT PS velocity vectors; **(b)** diagrams of the ERS/ENVISAT velocity values for the PS located within the hollow boundaries and indication of both the computed hollow velocity and the movement threshold; tilting of a masonry building and highlights on the crack pattern recorded during the surveys of 2000 **(c–d)** and 2012 **(e–g)**.

Assuming that a landslide is covered by a number of PS equal to N, the generic ith PS is characterized by a V_{LOS_i} value having an inaccuracy σ typically ranging from 1.5 to 2 mm yr^{-1} (Cascini et al., 2010; Cigna et al., 2012) depending on PS coherence. Accordingly, the portion of the landslide body referred to this PS can be assumed as moving if

$$V_{\mathrm{los}_i}^2 > \sigma^2. \tag{A1}$$

Considering that different PS on a landslide may exhibit different coherence values, a movement indicator – representative of the whole landslide – to be compared with the threshold can be individuated from slope measurements according to the equation:

$$\sum_{i=1}^{N} w_i \frac{V_{\mathrm{slope}_i}^2}{k_i^2} > \sigma^2 \tag{A2}$$

being $w_i = w_{ci}/w_{cN}$ the normalized weights based on the PS coherence and $k_i (\geq 1)$ the point-dependent V_{LOS} to V_{slope} scaling factor.

Letting $V_{\mathrm{slope\_rms}}$ be

$$V_{\mathrm{slope\_rms}} = \left(\sum_{i=1}^{N} w_i \, V_{\mathrm{slope\_i}}^2 \right)^{1/2} \tag{A3}$$

starting from Eqs. (A2) and (A3), a final test in terms of $V_{\mathrm{slope\_rms}}$ referring to the whole landslide, can be derived as

$$\frac{1}{k^2} V_{\mathrm{slope\_rms}}^2 > \sigma^2, \tag{A4}$$

where $k = \left(\frac{1}{N} \sum_{i=1}^{N} k_i^{-2} \right)^{-1/2} > 1$ represents the root mean square (rms) scaling factor to be used to account for the instrumental inaccuracy.

Finally, from Eq. (A4)

$$V_{\mathrm{slope\_rms}} > k\sigma. \tag{A5}$$

Equation (A5) shows that the landslide moving threshold on the rms velocity along the slope ($V_{\mathrm{slope\_rms}}$) must take into account that the inaccuracy due to instrumental error should be properly amplified according to the scaling factor k depending, in turn, on the landslide aspect and slope as well as on the sensor LOS. It is worth noting that Eqs. (A2) and (A4) are equivalent if and only if the scaling factors k_i have a constant value ($k_i = k$); however, Eq. (A5) has the advantage of including parameters (a slope velocity rms and scaling factor) relevant to the whole landslide.

Acknowledgements. The Authors are grateful to the National Basin Authority of Liri-Garigliano and Volturno rivers, and in particular to the general secretary Vera Corbelli, for furnishing all the thematic maps and the damage survey fact sheets of the study area.

The Authors wish also to thank Italian Ministry of the Environment and Protection of Land and Sea, and in particular Salvatore Costabile, for providing the PSI data of the study area deriving from the Piano Straordinario di Telerilevamento Ambientale.

The work described in this paper was supported by the project SafeLand "Living with landslide risk in Europe: Assessment, effects of global change, and risk management strategies" under Grant Agreement No. 226479 in the 7th Framework Programme of the European Commission. This support is gratefully acknowledged.

Edited by: V. Tofani
Reviewed by: two anonymous referees

References

APAT: Rapporto sulle frane in Italia. Il progetto IFFI – Metodologia, risultati e rapporti regionali, Agenzia per la Protezione dell'Ambiente e per i Servizi Tecnici, ISBN 978-88-448-0310-0, 2007.

Berardino, P., Fornaro, G., Lanari, R., and Sansosti, E.: A New Algorithm for Surface Deformation Monitoring based on Small Baseline Differential SAR Interferograms, IEEE Trans. Geosci. Remote Sens., 40, 2375–2383, 2002.

Bertolini, G., Guida, M., and Pizzaiolo, M.: Landslides in Emilia-Romagna region (Italy): strategies for hazard assessment and risk management, Landslides, 2, 302–312, 2005.

Bianchini, S., Cigna, F., Righini G., Proietti, C., and Casagli, N.: Landslide HotSpot Mapping by means of Persistent Scatterer Interferometry, Environ. Earth Sci., 67, 1155–1172, 2012.

Bonnard, Ch., Tacher, L., and Beniston, M.: Prediction of landslide movements caused by climate change: modelling the behaviour of a mean elevation large slide in the Alps and assessing its uncertainties, in: Landslides and Engineered Slopes – From the past to the future, edited by: Chen Z., Zhang J., Li Z., Wu F., and Ho, K., Proceedings of the 10th International Symposium on Landslides and Engineered Slopes, 30 June-4 July 2008, Xi'an (China), CRC Press, 1, 217–227, 2008.

Budetta, P., Calcaterra, D., Crescenti, E., De Riso, R., Parise, M., and Santo, A: Fenomeni di instabilità nell'area compresa tra Pietraroia e Guardia Sanframondi (Campania), Geologia Applicata e Idrogeologia, 29, 19–43, 1994.

Cascini, L., Bonnard, Ch., Corominas, J., Jibson, R., and Montero-Olarte, J.: Landslide hazard and risk zoning for urban planning and development – State of the Art report, in: Landslide Risk Management, Proceedings of the International Conference on Landslide Risk Management, edited by: Hungr, O., Fell, R., Couture, R., and Eberhardt, E., 31 May–3 June 2005, Vancouver, Canada, A.A. Balkema Publishers, 199–235, 2005.

Cascini, L., Ferlisi, S., Peduto, D., Pisciotta, G., Di Nocera, S., and Fornaro, G.: Multitemporal DInSAR data and damage to facilities as indicators for the state of activity of slow-moving landslides, in: Landslides and Engineered Slopes – From the past to the future, edited by: Chen, Z., Zhang, J., Li, Z., Wu, F., and Ho, K., Proceedings of the 10th International Symposium on Landslides and Engineered Slopes, 30 June-4 July 2008, Xi'an (China), CRC Press, 2, 1103–1109, 2008.

Cascini, L., Fornaro, G., and Peduto, D.: Analysis at medium scale of low-resolution DInSAR data in slow-moving landslide-affected areas, ISPRS J. Photogram. Remote Sens., 64, 598–611, 2009.

Cascini, L., Fornaro, G., and Peduto, D.: Advanced low- and full-resolution DInSAR map generation for slow-moving landslide analysis at different scales, Eng. Geol., 112, 29–42, 2010.

Catani, F., Casagli, N., Ermini, L., Righini, G., and Menduni, G.: Landslide hazard and risk mapping at catchment scale 2005 Arno River basin, Landslides, 2, 329–342, 2005.

Cigna, F., Del Ventisette, C., Liguori, V., and Casagli, N.: Advanced radar-interpretation of InSAR time series for mapping and characterization of geological processes, Nat. Hazards Earth Syst. Sci., 11, 865—881, doi:10.5194/nhess-11-865-2011, 2011.

Cigna, F., Bianchini, S., and Casagli, N: How to assess landslide activity and intensity with Persistent Scatterer Interferometry (PSI): the PSI-based matrix approach, Landslides, 1–17, doi:10.1007/s10346-012-0335-7, 2012.

Colesanti, C. and Wasowski, J.: Investigating landslides with space-borne Synthetic Aperture Radar (SAR) interferometry, Eng. Geol., 88, 173–199, 2006.

Colesanti, C., Ferretti, A., Novali, F., Prati, C., and Rocca, F.: SAR Monitoring of progressive and seasonal round deformation using the permanent scatterers technique, IEEE Trans. Geosci. Remote Sens., 41, 1685–1701, 2003.

Costantini, M., Falco, S., Malvarosa, F., and Minati, F.: A new method for identification and analysis of persistent scatterers in series of SAR images, IEEE International Geoscience & Remote Sensing Symposium, July 6-11, 2008, Boston, Massachusetts, USA, 449–452, 2008.

Cotecchia, V.: The Second Hans Cloos Lecture. Experience Drawn from the Great Ancona Landslide of 1982, Bull. Eng. Geol. Environ., 65, 1–41, 2006.

Cotecchia, F., Santaloia, F., Bottiglieri, O., and Monterisi, L.: Landslides in stiff clay slopes along the Adriatic coast (Central Italy), in: Landslides and Engineered Slopes – From the past to the future, Proceedings of the 10th International Symposium on Landslides and Engineered Slopes, edited by: Chen, Z., Zhang, J., Li, Z., Wu, F., and Ho, K., 30 June–4 July 2008, Xi'an (China), CRC Press, 2, 1525–1531, 2008.

Crosetto, M., Biescas, E., and Duro, J.: Generation of advanced ERS and Envisat interferometric SAR products using the stable point network technique, Photogram. Eng. Remote Sens., 4, 443–450, 2008.

Cruden, D. M. and Varnes, D. J.: Landslides Types and Processes, in: Landslides: Investigation and Mitigation, edited by: Turner, A. K. and Schuster, R. L., Washington DC, Transportation Research Board, National Academy of Sciences, Special Report 247, 36–75, 1996.

D'Elia, B. and Rossi-Doria, M.: Slow movements of earthflow accumulations along the Ionic Coast (South-Eastern Italy), Landslides in research, theory and practice, in: Proceedings of the 8th International Symposium on Landslides, edited by: Bromhead, E., Dixon, N., and Ibsen, M.-L., 26–30 June 2000, Cardiff, UK, Thomas Telford, London, 1, 439–446, 2000.

D'Elia, B., Esu, F., Pellegrino, A., and Pescatore, T. S.: Some effects on natural slope stability induced by 1980 Italian earthquake, Proceedings of the 11th International Conference on Soil Mechanics and Foundation Engineering, San Francisco, 4, 1943–1949, 1985.

DORIS: available at: http://www.doris-project.eu, last access: 19 December 2012.

Fell, R., Corominas, J., Bonnard, Ch., Cascini, L., Leroi, E., and Savage, W. Z. on behalf of the JTC-1 Joint Technical Committee on Landslides and Engineered Slopes: Guidelines for landslide susceptibility, hazard and risk zoning for land use planning, Eng. Geol., 102, 85–98, 2008a.

Fell, R., Corominas, J., Bonnard, Ch., Cascini, L., Leroi, E., Savage, W. Z. on behalf of the JTC-1 Joint Technical Committee on Landslides and Engineered Slopes: Guidelines for landslide susceptibility, hazard and risk zoning for land-use planning, Commentary, Eng. Geol., 102, 99–111, 2008b.

Ferlisi, S. and Pisciotta, G.: A preliminary study of landslide induced property damages towards consequence analysis, in: Proceedings of the First North American Landslide Conference, edited by: Schuster, V. R., Schuster, R. L., Turner, A. K., Vail

(Colorado), 3–9 June 2007, AEG Publication n. 23, ISBN 978-0-975-4295-3-2, (on CD-ROM), 2007

Ferretti, A., Prati, C., and Rocca, F.: Nonlinear subsidence rate estimation using permanent scatterers in differential SAR interferometry, IEEE Trans. Geosci. Remote Sens., 38, 2202–2212, 2000.

Ferretti, A., Prati, C., and Rocca, F.: Permanent scatterers in SAR interferometry, IEEE Trans. Geosci. Remote Sens., 39, 8–20, 2001.

Fornaro, G., Pauciullo, A., and Serafino, F.: Deformation monitoring over large areas with multipass differential SAR interferometry: a new approach based on the use of spatial differences, Int. J. Remote Sens., 30, 1455–1478, 2009a.

Fornaro, G., Reale, D., and Serafino, F.: Four-dimensional SAR imaging for height estimation and monitoring of single and double scatterers, IEEE Trans. Geosci. Remote Sens., 47, 224–237, 2009b.

Fumagalli, A., Novali, F., Prati, C., Rocca, F., and Rucci, A.: A New Algorithm for Processing Interferometric Data-Stacks: SqueeSAR, IEEE Trans. Geosci. Remote Sens., 49, 3460–3470, 2011.

Guadagno, F. M., Focareta, M., Revellino, P., Bencardino, M., Grelle, M., Lupo, M., and Rivellini, G.: Carta delle frane della provincia di Benevento, Publication n°2906/2006 of GNDCI (U.O. 2.24 Resp. F.M. Guadagno), Sannio University Press, Benevento, 1–77, 2006.

Guzzetti, F., Ardizzone, F., Cardinali, M., Galli, M., and Reichenbach, P.: Distribution of landslides in the Upper Tiber River basin, central Italy, Geomorphology, 96, 105–122, 2008.

Guzzetti, F., Mondini, A. C., Cardinali, M., Fiorucci, F., Santangel, M., and Chang, K.-T.: Landslide inventory maps: New tools for an old problem, Earth-Sci. Rev., 112, 42–66, 2012.

Herrera, G., Notti, D., Garcia-Davalillo, J. C., Mora, O., Cooksley, G., Sanchez, M., Arnaud, A., and Crosetto, M.: Analysis with C- and X-band satellite SAR data of the Portalet landslide area, Landslides, 8, 195–206, 2011.

Herrera, G., Gutiérrez, F., García-Davalillo, J. C., Guerrero, J., Notti, D., Galve, J. P., Fernandez-Merodo, J. A., and Cooksley, G.: Multi-sensor advanced DInSAR monitoring of very slow landslides: The Tena Valley case study (Central Spanish Pyrenees), Remote Sens. Environ., 128, 31–43, 2013.

Leone, F., Asté, J. P., and Leroi, E.: Vulnerability assessment of elements exposed to mass-movement: Working toward a better risk perception, in: Landslides – Glissements de terrain, edited by: Senneset, K., Proceedings of the 7th International Symposium on Landslides, A.A. Balkema, 263–269, 1996.

Lu, P., Casagli, N., Catani, F., and Tofani, V.: Persistent Scatterers Interferometry Hotspot and Cluster Analysis (PSI-HCA) for detection of extremely slow-moving landslides, Int. J. Remote Sens., 33, 466–489, 2012.

Malamud, B. D., Turcotte, D. L., Guzzetti, F., and Reichenbach, P.: Landslide inventories and their statistical properties, Earth Surf. Process. Landf., 26, 687–711, 2004.

Mansour, M. F., Morgenstern, N. R., and Martin, C. D.: Expected damage from displacement of slow-moving slides, Landslides, 7, 117–131, 2011.

MATTM: Piano Straordinario di Telerilevamento Ambientale (PST-A), Linee guida per l'analisi dei dati intereferometrici satellitari in aree soggette a dissesti idrogeologici, Italian Ministry of the Environment and Protection of Land and Sea (MATTM), 108 pp., 2010.

Meisina, C., Zucca, F., Notti, D., Colombo, A., Cucchi, A., Savio, G., Giannico, C., and Bianchi, M.: Geological Interpretation of PSInSAR Data at Regional Scale, Sensors 2008, 8, 7469–7492, 2008.

Melidoro, G.: Movimenti franosi e zonizzazione del bacino del fiume Fortore, Geologia Applicata e Idrogeologia, 6, 7–41, 1971.

Nichol, J., and Wong, M. S: Satellite remote sensing for detailed landslide inventories using change detection and image fusion, Int. J. Remote Sens., 26, 1913–1926, 2005.

Notti, D., Davalillo, J. C., Herrera, G., and Mora, O.: Assessment of the performance of X-band satellite radar data for landslide mapping and monitoring: Upper Tena Valley case study, Nat. Hazards Earth Syst. Sci., 10, 1865–1875, doi:10.5194/nhess-10-1865-2010, 2010.

Picarelli, L. and Russo, C.: Remarks on the mechanics of slow active landslides and the interaction with man-made works, in: Landslides – Evaluation & Stabilization, edited by: Lacerda, W. A., Ehrlich, M., Fontoura, S. A. B., and Sayão, A. S. F., Proceedings of the 9th International Symposium on Landslides, 28 June–2 July 2004, Rio de Janeiro, A.A. Balkema Publishers, 2, 1141–1176, 2004.

Pisciotta, G.: Physical vulnerability of element at risk in landslide prone areas, PhD Thesis, University of Salerno, Italy, 270 pp., 2008.

Plank, S., Singer, J., Minet, Ch., and Thuro, K.: GIS based suitability evaluation of the differential radar interferometry method (D-InSAR) for detection and deformation monitoring of landslides, in: Proceedings of Fringe 2009 Workshop, edited by: Lacoste-Francis, H., 30 November–4 December 2009, ESRIN, Frascati, Italy (ESA SP-677, March 2010), 8 pp., ISBN: 978-92-9221-241-4, 2010.

Rapolla, A., Di Nocera, S., Matano, F., Paoletti, V., and Tarallo, D: Le aree dei terreni complessi del Sannio e dell'Irpinia, in: Criteri di zonazione della suscettibilità e della pericolosità da frane innescate da eventi estremi (piogge e sisma), Composervice S.r.l., Padova, Italy, 238–248, ISBN: 9788890687334, 2012.

Righini, G., Pancioli, V., and Casagli, N.: Updating landslide inventory maps using Persistent Scatterer Interferometry (PSI), Int. J. Remote Sens., 33, 2068–2096, 2012.

Risknat Project: in: Le tecniche radar interferometriche nella pianificazione territoriale, KC Edizioni, Genova, Italy, 188 pp., ISBN: 978-88-89007-37-2, 2012.

SafeLand Deliverable 4.4.: Guidelines for the selection of appropriate remote sensing technologies for monitoring different types of landslides, edited for the SafeLand European project by: Stumpf, A., Malet, J.-P., and Kerle, N., available at: http://www.safeland-fp7.eu (last access: 23 May 2013), 2011.

SCAI Project: in: Studio dei centri abitati instabili della Regione Campania, edited by: De Riso, R., Di Nocera, S., and Pescatore, T. S., Giannini Editore, Naples, Italy, ISBN: 88-7431-257-1, 2004.

Soeters, R. and van Westen, C. J.: Slope instability recognition, analysis and zonation, in: Landslides Investigation and Mitigation, edited by: Turner, A. K. and Schuster, R. L., TRB Special Report 247, National Academy Press, Washington DC, 129–177, 1996.

Spizzichino, D., Falconi, L., Delmonaco, G., Margottini, C., and Puglisi, C.: Integrated approach for landslide risk assessment of Crago Village (Italy), in: Landslides – Evaluation & Stabilization, edited by: Lacerda, W. A., Ehrlich, M., Fontoura, S. A. B., and Sayão, A. S. F., Proceedings of the 9th International Symposium on Landslides, 28 June–2 July 2004, Rio de Janeiro, A.A. Balkema Publishers, 1, 237–242, 2004.

TERRAFIRMA: available at: http://www.terrafirma.eu.com, last access: 1 December 2012.

Terranova, C., Iuliano, S., Matano, F., Nardò, S., Piscitelli, E., Cascone, E., D'Argenio, F., Gelli L., Alfinito, M., and Luongo, G.: The TELLUS Project: a satellite-based slow-moving landslides monitoring system in the urban areas of Campania Region, Proceedings of the Conference on Geology and Information Technology, 3–5 June 2008, Offida (AP), Rendiconti On line della Società Geologica Italiana, 8, 148–151, 2009.

Tofani, V., Segoni, S., Agostini, A., Catani, F., and Casagli, N.: Technical Note: Use of remote sensing for landslide studies in Europe, Nat. Hazards Earth Syst. Sci., 13, 299–309, doi:10.5194/nhess-13-299-2013, 2013.

Urciuoli, G. and Picarelli, L.: Interaction between landslides and man-made works, in: Chen Z., Zhang J., Li Z., Wu F., Ho K. (eds.), Landslides and Engineered Slopes – From the past to the future. Proceedings of the 10th International Symposium on Landslides and Engineered Slopes, 30 June–4 July 2008, Xi'an (China), CRC Press, 2, 1301–1307, 2008.

Van den Eeckhout, M., Poesen, J., Verstraeten, G., Vanacker, V., Nyssen, J., Moeyersons, J., Van Beek, L. P., and Vandekerckhove, L.: Use of LIDAR-derived images for mapping old landslides under forest, Earth Surf. Process. Landf., 32, 754–769, 2007.

van Westen, C. J.: Geo-Information tools for landslide risk assessment: an overview of recent developments, in: Landslides – Evaluation & Stabilization, edited by: Lacerda, W. A., Ehrlich, M., Fontoura, S. A. B., and Sayão, A. S. F., Proceedings of the 9th International Symposium on Landslides, 28 June–2 July 2004, Rio de Janeiro, A.A. Balkema Publishers, 1, 39–56, 2004.

van Westen, C. J., Castellanos, E., and Kuriakose, S. L.: Spatial data for landslide susceptibility, hazards and vulnerability assessment: An overview, Eng. Geol., 102, 112–131, 2008.

Varnes, D. J.: Slope Movement Types and Processes, in: Special Report 176: Landslides: Analysis and Control, edited by: Schuster, R. L. and Krizek, R. J., TRB, National Research Council, Washington, DC, 11–33, 1978.

Wang, F. W., Wang, G., Zhang, Y. M., Huo, Z. T., Peng, X. M., Araiba, K., and Takeuchi, A.: Displacement Monitoring on Shuping Landslide in the Three Gorges Dam Reservoir Area, China from August 2004 to July 2007, in: Landslides and Engineered Slopes – From the past to the future. Proceedings of the 10th International Symposium on Landslides and Engineered Slopes, edited by: Chen, Z., Zhang, J., Li, Z., Wu, F., and Ho, K., 30 June–4 July 2008, Xi'an (China), CRC Press, 2, 1321–1327, 2008.

Wei, M. and Sandwell, D. T.: Decorrelation of L-band and C-band interferometry over vegetated areas in California, IEEE Trans. Geosci. Remote Sens., 48, 2942–2952, 2010.

Wieczoreck, G. F.: Preparing a detailed landslide-inventory map for hazard evaluation and reduction, Bull. Assoc. Eng. Geol., 21, 337–342, 1984.